

LA-UR-17-23552 (Accepted Manuscript)

Comparing simulated and observed EMIC wave amplitudes using in situ Van Allen Probes' measurements

Saikin, A.; Jordanova, Vania Koleva; Zhang, Jichun; Smith, C. W.; Spence, Harlan E.; Larsen, Brian Arthur; Reeves, Geoffrey D.; Torbert, R.; Kletzing, C.; Zhelavskaya, I.; Shprits, Y.

Provided by the author(s) and the Los Alamos National Laboratory (2018-02-14).

To be published in: Journal of Atmospheric and Solar-Terrestrial Physics

DOI to publisher's version: 10.1016/j.jastp.2018.01.024

Permalink to record: http://permalink.lanl.gov/object/view?what=info:lanl-repo/lareport/LA-UR-17-23552

Disclaimer

Approved for public release. Los Alamos National Laboratory, an affirmative action/equal opportunity employer, is operated by the Los Alamos National Security, LLC for the National Nuclear Security Administration of the U.S. Department of Energy under contract DE-AC52-06NA25396. Los Alamos National Laboratory strongly supports academic freedom and a researcher's right to publish; as an institution, however, the Laboratory does not endorse the viewpoint of a publication or guarantee its technical correctness.



Accepted Manuscript

Comparing simulated and observed EMIC wave amplitudes using *in situ* Van Allen Probes' measurements

A.A. Saikin, V.K. Jordanova, J.C. Zhang, C.W. Smith, H.E. Spence, B.A. Larsen, G.D. Reeves, R.B. Torbert, C.A. Kletzing, I.S. Zhelavskaya, Y.Y. Shprits

PII: \$1364-6826(17)30212-2

DOI: 10.1016/j.jastp.2018.01.024

Reference: ATP 4781

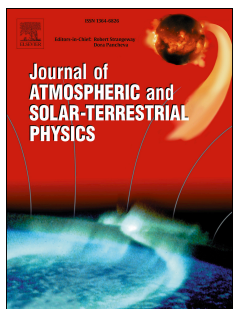
To appear in: Journal of Atmospheric and Solar-Terrestrial Physics

Received Date: 3 April 2017

Revised Date: 15 January 2018 Accepted Date: 18 January 2018

Please cite this article as: Saikin, A.A., Jordanova, V.K., Zhang, J.C., Smith, C.W., Spence, H.E., Larsen, B.A., Reeves, G.D., Torbert, R.B., Kletzing, C.A., Zhelavskaya, I.S., Shprits, Y.Y., Comparing simulated and observed EMIC wave amplitudes using *in situ* Van Allen Probes' measurements, *Journal of Atmospheric and Solar-Terrestrial Physics* (2018), doi: 10.1016/j.jastp.2018.01.024.

This is a PDF file of an unedited manuscript that has been accepted for publication. As a service to our customers we are providing this early version of the manuscript. The manuscript will undergo copyediting, typesetting, and review of the resulting proof before it is published in its final form. Please note that during the production process errors may be discovered which could affect the content, and all legal disclaimers that apply to the journal pertain.



1 2	Title: Comparing simulated and observed EMIC wave amplitudes using <i>in situ</i> Van Allen Probes' measurements
3 4 5	Authors: A. A. Saikin ^a (<u>aax75@wildcats.unh.edu</u>), V. K. Jordanova ^b , J. –C. Zhang ^a , C. W. Smith ^a , H. E. Spence ^a , B. A. Larsen ^{b,c} , G. D. Reeves ^{b,c} , R. B. Torbert ^a , C. A. Kletzing ^d , I. S. Zhelavskaya ^e , and Y. Y. Shprits ^{e,f}
6	
7	
8	
9	
10	
11 12	^a Space Science Center and Department of Physics, University of New Hampshire, Durham, NH 03824, USA
13	^b Los Alamos National Laboratory, Los Alamos, NM 87545, USA
14	^c The New Mexico Consortium, Los Alamos, NM 87544, USA
15	^d Department of Physics and Astronomy, University of Iowa, Iowa City, IA 52242, USA
16 17	^e Department of Earth, Planetary, and Space Sciences, University of California, Los Angeles, California, USA
18 19	^f Helmholtz Centre Potsdam, GFZ German Research Centre For Geosciences and University of Potsdam, Potsdam, Germany
20	
21	
22	Mailing address ^a :
23	8 College Road, Morse Hall, SSC, Durham, NH, 03824, USA
24	
25	
26	
27	

28	
29	Highlights:
30	• <i>In situ</i> plasma measurements cannot reproduce observed EMIC wave amplitudes.
31	• Inner magnetosphere A_{hp} distributions are asymmetric in MLT.
32	• A_{hp} decreases in the presence of EMIC waves.
33	• A_{hp} provides more "free energy" than A_{hhe} or A_{ho}
34	• A_{hp} must be increased (2 – 4 times measured value) to replicate EMIC wave amplitudes.
35	
36	
37	
38	
39	
40	
41	
42	
43	
44	
45	Key Words:
46	EMIC waves, Van Allen Probes, linear theory, Wave generation

Abstract:

We perform a statistical study calculating electromagnetic ion cyclotron (EMIC)
wave amplitudes based off in situ plasma measurements taken by the Van Allen Probes'
(1.1 to 5.8 R _e) Helium, Oxygen, Proton, Electron (HOPE) instrument. Calculated wave
amplitudes are compared to EMIC waves observed by the Electric and Magnetic Field
Instrument Suite and Integrated Science on board the Van Allen Probes during the same
period. The survey covers a 22-month period (1 November 2012 to 31 August 2014), a
full Van Allen Probe magnetic local time (MLT) precession. The linear theory proxy was
used to identify EMIC wave events with plasma conditions favorable for EMIC wave
excitation. Two hundred and thirty-two EMIC wave events (103 H ⁺ -band and 129 He ⁺ -
band) were selected for this comparison. Nearly all events selected are observed beyond
L = 4. Results show that calculated wave amplitudes exclusively using the <i>in situ</i> HOPE
measurements produce amplitudes too low compared to the observed EMIC wave
amplitudes. Hot proton anisotropy (A_{hp}) distributions are asymmetric in MLT within the
inner ($L < 7$) magnetosphere with peak (minimum) A_{hp} , ~0.81 to 1.00 (~0.62), observed
in the dawn (dusk), $0000 < MLT \le 1200$ ($1200 < MLT \le 2400$), sectors. Measurements
of A_{hp} are found to decrease in the presence of EMIC wave activity. A_{hp} amplification
factors are determined and vary with respect to EMIC wave-band and MLT. He ⁺ -band
events generally require double (quadruple) the measured A_{hp} for the dawn (dusk) sector
to reproduce the observed EMIC wave amplitudes.

1. Introduction

Electromagnetic ion cyclotron (EMIC) waves are Pc 1-2 pulsations (0.1 – 5 Hz) that play an integral role in manipulating particle dynamics within the Earth's magnetosphere. Through wave-particle interactions, EMIC waves may: scatter relativistic electrons (Jordanova et al., 2008; Lyons et al., 1972; Meredith et al., 2003; Thorne and Kennel, 1971), cause ring current protons to precipitate (Burch et al., 2002; Jordanova et al., 2001; Usanova et al., 2010; Xiao et al., 2012, 2011), and heat heavy ions (Zhang et al., 2011, 2010). EMIC waves have also been associated with the appearance of isolated auroral arc events (Sakaguchi et al., 2008), cusp proton aurora events (Xiao et al., 2013), and traveling convection vortices in the Earth's magnetosphere (Engebretson et al., 2013; Lockwood et al., 1990).

EMIC waves are generated when hot (10-100 keV) anisotropic $(T_{\perp}/T_{\parallel} > 1)$ ions (usually H⁺) overlap with cold dense plasma populations (Cornwall, 1965; Kennel and Petschek, 1966). The hot anisotropic ion populations provide the "free energy" necessary for EMIC wave growth (Cornwall, 1965; Rauch and Roux, 1982). The presence of cold heavy ions (i.e., He⁺ and O⁺) influence the formation of EMIC waves by enhancing the wave growth rate and lowering the threshold for the EMIC instability (Horne and Thorne, 1993; Rauch and Roux, 1982; Young et al., 1981). The impact of cold dense plasma populations on EMIC wave enhancement causes frequent suggestions that the plasmapause and plasmaspheric plumes are the favorable regions for EMIC wave excitation (Fraser et al., 1989; Morley et al., 2009; Usanova et al., 2013; Zhang et al.,

2010). Usanova et al. (2013) found EMIC waves to be ~20 times more likely to have been observed inside a plasmaspheric plume than outside

93

94

95

96

97

98

99

100

101

102

103

104

105

106

107

108

109

110

111

112

113

114

115

While EMIC wave events can be observed in any magnetic local time (MLT) sector, they are most frequently observed in the afternoon (1200 < MLT ≤ 1800) MLT sector (e.g., Anderson et al., 1992; Halford et al., 2010; Min et al., 2012; Usanova et al., 2012; Keika et al., 2013; Saikin et al., 2015, 2016; Paulson et al., 2016). The afternoon sector coincides with the well-established EMIC wave enhancement region (Thorne, 2010). EMIC waves within this region coincide with cold plasmaspheric plumes (Fraser and Nguyen, 2001) and hot ring current ion injections from the plasma sheet caused by disturbed geomagnetic conditions. During geomagnetic storms, hot ring current ions are injected into the inner (L < 7) magnetosphere, overlapping with these cold dense plasma populations, leading to EMIC wave generation (Cornwall, 1965; Criswell, 1969; Fraser et al., 2010; Jordanova et al., 2001; Saikin et al., 2016). Previous surveys revealed the EMIC wave occurrence rates increase during geomagnetic storm phases (Halford et al., 2016; Saikin et al., 2016), increasing values of Kp (Kasahara et al., 1992), and disturbed (AE > 300 nT) geomagnetic conditions (Meredith et al., 2014; Saikin et al., 2016; Usanova et al., 2012). Magnetospheric compressions are often considered a cause of outer magnetosphere EMIC wave generation (Allen et al., 2015; Anderson and Hamilton, 1993; Usanova et al., 2012) with particles executing Shabansky orbits to help generate the necessary anisotropy (McCollough et al., 2012; Shabansky, 1971).

Excited with a left-hand polarization, these transverse propagating waves are preferably generated in regions of low magnetic field strength (Kennel and Petschek, 1966). Generally, these source regions are confined to the magnetic equator within $\pm 10^{\circ}$

magnetic latitude (MLAT) (Loto'aniu et al., 2005). However, evidence of off-equator EMIC wave generation has been observed (Allen et al., 2013, 2016). Post generation, EMIC waves propagate along field lines to regions of increased magnetic field strength (Mauk and McPherron, 1980).

EMIC waves can be classified with respect to the wave-band within which they occur. Wave activity observed below the proton gyrofrequency (denoted as $f(H^+)$) and above the helium ion gyrofrequency ($f(He^+)$) are classified as proton-band (H^+ -band) EMIC waves. Similarly, events found between the $f(He^+)$ and the oxygen ion gyrofrequency ($f(O^+)$) are known as helium-band (He^+ -band) EMIC waves. Varying the heavy ion concentration present during EMIC wave generation directly impacts which wave-bands become excited (Kozyra et al., 1984). For example, the presence of cold He^+ increases the growth rate for He^+ -band EMIC waves, while lowering the growth rate for H^+ -band EMIC waves (Kozyra et al., 1984). Furthermore, wave-band specific EMIC waves are not observed equally (Keika et al., 2013; Min et al., 2012; Saikin et al., 2015; Wang et al., 2015; Yu et al., 2015). Consistently, He^+ -band EMIC waves have higher wave powers than their H^+ - or O^+ -band counterparts (Horne and Thorne, 1993), particularly in the afternoon sector (Min et al., 2012; Saikin et al., 2015).

EMIC waves remain an important topic of discussion given their role in particle dynamics and cross-energy plasma interactions within the Earth's magnetosphere.

Numerous statistical studies on EMIC wave observation using *in situ* measurements (e.g., Allen et al., 2015; Anderson et al., 1992; Halford et al., 2010; Kasahara et al., 1992; Keika et al., 2013; Min et al., 2012; Saikin et al., 2015; Usanova et al., 2012) and simulations calculating EMIC wave growth rates (e.g., Rauch and Roux, 1982; Kozyra et

al., 1984; Horne and Thorne, 1993; Jordanova et al., 2001, 2007; Denton et al., 2014;
Gamayunov et al., 2014) have been performed over the years. Statistical in situ
observations, while generally consistent, possess orbital biases dependent upon which
mission is used (Saikin et al., 2015). Similarly, different EMIC wave simulation studies
examine alternate magnetospheric locations (e.g., $L=4$ - 7 (Horne and Thorne, 1993), L
= 3 - 6 (Gamayunov et al., 2014)), with plasmaspheric enhancements used when
necessary (Jordanova et al., 2001; Kozyra et al., 1984), and focus on either EMIC wave
generation (e.g., Bortnik et al., 2011; Omidi et al., 2011; Fu et al., 2016) and/or EMIC
wave propagation (e.g., Roux et al., 1982; Horne and Thorne, 1993; Khazanov and
Gamayunov, 2007; Gamayunov et al., 2014) . Common parameters investigated in these
parametric simulation studies include the anisotropy of hot protons, parallel plasma beta,
the density of hot protons, and the concentration of cold plasma (Bortnik et al., 2011; Fu
et al., 2016; Gamayunov et al., 2014; Kozyra et al., 1984). While metrics exist that
examine the in situ plasma conditions associated with EMIC waves to determine if wave
activity is possibly observed within the source region (Allen et al., 2016; Blum et al.,
2009; Gary et al., 1994; Zhang et al., 2014), these measurements are generally not used in
conjunction with simulations to reproduce the observed EMIC waves.

Recent studies have attempted to derive the relationship between initial plasma conditions and the saturation amplitude of EMIC waves. 2-D hybrid simulations performed by Bortnik et al. (2011) revealed that the saturation of EMIC wave amplitudes increase monotonically when hot proton densities and anisotropies are increased (i.e., increased linear growth). Another study derived a relationship between EMIC wave saturation and parameters associated with the linear theory proxy (Fu et al., 2016). Both

studies are purely theoretical and do not use *in situ* plasma measurements. To our knowledge, a study focusing on replicating observed EMIC wave amplitudes with *in situ* plasma measurements has not been performed.

In this study, we seek to expand upon the work by Bortnik et al. (2011) and Fu et al. (2016) by calculating EMIC wave amplitudes with parameters set up according to *in situ* plasma measurements. This study will be performed using data taken by the Van Allen Probes over a 22-month period, a full MLT precession, and with EMIC wave calculations based off the work by Jordanova et al. (2001). This paper will be organized as follows: a description of the Van Allen Probes and the instruments used (section 2.1), the selection of EMIC wave events and EMIC wave favorable plasma conditions (section 2.2 and 2.3, respectively), an explanation of the model used to calculate wave growth rates (section 2.4), results on how the calculations compare to the Van Allen Probes' observations (section 3), and finally, a discussion and conclusions (section 4 and 5, respectively).

2. Methodology

2.1 Van Allen Probes

The Van Allen Probes mission (Kessel et al., 2013; Mauk et al., 2013) are two identical spacecraft that orbit around the Earth with an apogee and perigee of 5.8 and 1.1 R_e , respectively. Each probe performs a highly elliptical, low inclination (~10°) orbit with a period of ~9 h. The probes, denoted as Probe A and Probe B, follow nearly identical orbits at different speeds, causing one probe to lap the other every ~2.5 months. The perigee-apogee line of each probe precess in local time at a rate of ~210°/yr.

For this study, two instruments on board both Van Allen Probes have been used to
identify EMIC wave activity and measure the plasma conditions during their
observations. The Electric and Magnetic Field Instrument Suite and Integrated Science
(EMFISIS) (Kletzing et al., 2013) contains a magnetometer instrument that provides high
temporal resolution (64 vectors per second) magnetic field measurements. EMFISIS
instrument suite has two magnetic field sensors, a triaxial fluxgate magnetometer (MAG),
and a triaxial AC magnetic search coil magnetometer. For this study, we have only used
magnetic field measurements from MAG. Electron density (n_e) was determined using the
Neural-network-based Upper hybrid Resonance Determination (NURD) algorithm
developed by Zhelavskaya et al. (2016). The authors employed feedforward neural
networks to reconstruct the upper hybrid frequency from plasma wave observations made
on board the Van Allen Probes. The inputs to the NURD neural network are the EMFISIS
High Frequency Receiver observations and geophysical parameters and the output is the
upper hybrid frequency. After training and validating the NURD model for 1,091 Van
Allen Probes orbits, it was used to estimate the upper hybrid frequency (and by extension,
the electron density) for all Van Allen Probe orbits for the period of 1 October 2012 to 1
July 2016 (Zhelavskaya et al., 2016). The resulting electron density data set is available
on the ftp server: ftp://rbm.epss.ucla.edu/ftpdisk1/NURD/ EMIC wave amplitudes were
calculated following the procedure established in previous studies (Allen et al., 2015;
Saikin et al., 2015). A fast Fourier transform technique (FFT) analysis was performed on
the high resolution magnetic field data taken by the EMFISIS instrument for each EMIC
wave. A 10-second mean magnetic field was utilized as the background field from which
the magnetic field data were rotated from GSE coordinates to field-aligned coordinates.

This FFT wave analysis used 4096 steps with an input step length of 512 points, and was applied to this field-aligned data.

Plasma data were obtained from the Helium, Oxygen, Proton, and Electron (HOPE) mass spectrometer (Funsten et al., 2013), which is part of the Radiation Belt Storm Probes-Energetic Particle Composition and Thermal Plasma (RBSP-ECT) Suite (Spence et al., 2013). The HOPE mass spectrometer measures electron and ion flux distributions over 4π sr every spacecraft spin in the energy range of ~1 eV – 52 keV with a ~12 second cadence. HOPE also distinguishes between the three major ion species of H⁺, He⁺, and O⁺. Available data from the HOPE instrument begin on 25 October 2012. This EMIC wave survey encompasses the period of 1 November 2012 – 31 August 2014. This 22-month period covers one complete Van Allen Probes MLT precession.

2.2 EMIC Wave selection method

EMIC wave selection follows the same guidelines described in Saikin et al. (2015) and Saikin et al. (2016). EMIC wave events were visually identified from daily plots generated from the EMFISIS data set. EMIC wave events must be observed for at least 5 minutes in Universal Time (UT). This time limit was imposed to avoid background noise being considered EMIC wave activity. Furthermore, broadband ultra low frequency (ULF) wave activity was not included in this study (for an example, see Figure 1c in Zhang et al. (2014) of broadband and EMIC wave activity). A minimum wave power threshold of 0.01 nT²/Hz was employed, with wave power being calculated by the procedures described in Allen et al. (2013) and Zhang et al. (2014). H⁺- and He⁺- band EMIC wave events have been included in this study. O⁺-band EMIC wave events,

while observed by the Van Allen Probes, were not included in this study given their low occurrence rates (Saikin et al., 2015; Yu et al., 2015).

2.3 Linear theory proxy

Not all H⁺- and He⁺-band EMIC wave events observed within this 22-month precession were used in this study. Since the purpose of this study is to use *in situ* plasma measurements to replicate the observed EMIC wave amplitudes, only EMIC wave events observed when plasma conditions were favorable for EMIC wave excitation were used for our analysis. This event selection was determined by testing the Van Allen Probes' EMIC wave observations with a linear theory proxy. Derived assuming an electron-proton collisionless plasma where both species are represented with bi-Maxwellian velocity distributions, linear theory states that if the observational growth parameter, Σ_h , exceeds the theoretical instability threshold, S_h , then the plasma is favorable for EMIC wave excitation (Blum et al., 2009; Gary et al., 1994; Zhang et al., 2014). Events with any plasma conditions that satisfied this criterion, $\Sigma_h - S_{\square} > 0$, for at least a 1 minute UT duration were included in this study. Here, the observational growth parameter is defined as:

$$\Sigma_h = \left(\frac{T_\perp}{T_\parallel} - 1\right) \beta_{\parallel hp}^{\alpha_h}$$

$$\alpha_h = a_0 - a_1 \ln \left(\frac{n_{hp}}{n_e}\right) - a_2 \left[\ln \left(\frac{n_{hp}}{n_e}\right)\right]^2$$

The observational growth parameter depends explicitly on the hot ($\geq 1 \text{ keV}$) proton anisotropy, $A_{hp} = T_{\perp}/T_{\parallel} - 1$, the parallel hot proton plasma beta, $\beta_{\parallel hp}$, and the ratio of the hot proton to electron density, n_{hp}/n_e . The hot proton data was extracted

from the HOPE instrument measurements and covers the 1-52 keV energy channels. "Hot" was defined as ≥ 1 keV since enhancements in proton energy flux can begin at ~1 keV (for an example proton energy flux spectrum, see Figure 3 in Zhang et al. (2014)). For consistency, each linear theory proxy calculation used the same "hot" proton definition. The constants a_0 , a_1 , and a_2 are derived from Blum et al. (2009), and equal 0.409, 0.0145, and 0.00028, respectively.

The theoretical instability threshold is defined as:

$$S_h = \sigma_0 + \sigma_1 \ln \left(\frac{n_{hp}}{n_e} \right) + \sigma_2 \left[\ln \left(\frac{n_{hp}}{n_e} \right) \right]^2$$

Here, $\sigma_0=0.429$, $\sigma_1=0.124$, and $\sigma_2=0.0018$. These values are also derived by Blum et al. (2009).

2.4 Calculating EMIC wave amplitudes

To calculate EMIC wave convective growth rates, this study follows the procedures outlined by Koyzra et al. (1984) and Jordanova et al. (2001). Given that EMIC wave amplification depends on the time spent within the source region, convective growth rates are more suitable for understanding EMIC wave growth. Convective growth rates were obtained from the hot plasma dispersion relation using ring current H^+ , He^+ , and O^+ densities, parallel energy (T_1), and anisotropy (A_h) measurements taken by the HOPE instrument. The calculation considers frequencies between f(H+) and f(O+), and selects the maximum convective growth rate per wave band. Local growth rates are then integrated along wave paths, which are field-aligned and extend over $\pm 5^{\circ}$ MLAT to get the wave gain G (decibels). The presence of plasmaspheric cold plasma populations is included in the calculation. For the calculation, H^+ -band EMIC wave events were

assumed to have a H⁺ rich cold plasma concentration: 100% H⁺, 0% He⁺, and 0% O⁺. He⁺-band EMIC wave events were presumed to have a more varied cold plasma concentration: 77% H⁺, 22% He⁺, and 3% O⁺. These different cold plasma concentrations were chosen since wave-band specific EMIC wave growth rates are heavily dependent on the concentrations of heavy ions in a cold plasma (Kozyra et al., 1984). Events located near the plasmapause (or within 0.25 R_E on either side) received an extended ±10° (±7.5°) MLAT wave path. This cold plasmaspheric enhancement factor is based on the guiding of waves along the plasmapause, i.e. the thermal density gradient allows the wave vector to remain field aligned and wave growth is possible over a longer ray path (Jordanova et al., 2001; Thorne and Horne, 1997) The convective growth rate, S (1/cm), is calculated by taking the ratio of the temporal growth rate, μ (1/s), and the group velocity, V_g (cm/s) (Kozyra et al., 1984):

$$S = \frac{\mu}{V_a}$$

The temporal growth rate is determined by:

$$\mu = \frac{\omega_{i}}{\Omega_{p}}$$

$$= \left\{ \sum_{i} \frac{\Omega_{p} \eta_{lw} \sqrt{\pi}}{M_{i}^{2} \alpha_{ll} k} \left[[(A_{i} + 1)(1 - M_{i}X) - 1] * exp \left[\frac{-\Omega_{p}^{2}}{M_{i}^{2}} \frac{(M_{i}X - 1)^{2}}{\alpha_{ll}^{2} k^{2}} \right] \right] \right\}$$

$$* \left\{ \frac{X(\delta + 1)(2 - X)}{(X - 1)^{2}} + \sum_{j} (\eta_{jw} + \eta_{jc}) * \frac{M_{j}X(2 - M_{j}X)}{(M_{j}X - 1)^{2}} \right\}^{-1}$$

$$M_j = \frac{m_j}{z_j m_p}$$
, $\eta_{jw(c)} = M_j \frac{\omega_{pwj(c)}^2}{\omega_{ppw}^2}$

The temporal growth depends on the plasma frequency for that respective ion (j) and warm (cold) population, $\omega_{pjw(c)}$, the real part of the frequency, ω_r , the mass of the ion species, m_i , the proton gyrofrequency, Ω_p .

The group velocity is determined by:

$$V_g = \frac{\partial \omega}{\partial k} = \left\{ \frac{2\Omega_p c}{\omega_{ppw}} \left[\frac{1+\delta}{1-X} + \sum_j \eta_{jw} + \eta_{jc} \frac{M_j}{1+M_j X} \right]^{\frac{1}{2}} \right\} *$$

$$\left\{ \frac{(1+\delta)(2-X)}{(1-X)^2} + \sum_{j} \frac{(\eta_{jw} + \eta_{jc})M_j(2-M_jX)}{(1-M_jX)^2} \right\}^{-1}$$

With the maximum convective growth rate determined, the gain [dB] for that convective growth rate was calculated. Following the procedure described in Kozyra et al. (1997), the maximum wave gain was related to the maximum EMIC wave amplitude, via a simple model, and the gain was then used to calculate the max wave amplitude, B_w : $B_w = 10 * 10^{\frac{G-G_1}{20}}$ (nT). For best agreement with the data, $G_1 = 40$ (Jordanova et al., 2001).

3. Results

3.1 Linear theory observations

Following the criteria established in Section 2.2 and 2.3, 628 EMIC wave events were initially identified between 1 November 2012 and 31 August 2014. Each event was examined with the linear theory proxy to determine if their observations coincided with favorable plasma conditions for EMIC wave excitation.

Figure 1 shows a sample He ⁺ -band EMIC wave event (panel a) and its
corresponding linear theory proxy calculation as observed by Van Allen Probe-A on 25
May 2013 between 1705 – 1715 UT. All the plasma parameters associated with linear
theory, as described above, are featured in Figure 1. During the 25 May 2013 EMIC wave
event, marked by the green translucent rectangle, A_{hp} (panel b) remains at relatively high
values ($A_{hp} = \sim 0.70$ to ~ 0.90). This wave activity also coincides with steep enhancements
in both β_{lhp} (panel c) and n_{hp} (panel d). Before and during the EMIC wave activity, n_e
(panel e) steadily decreases, indicating that Van Allen Probe-A is probably in the process
of leaving the post-dusk plasmasphere. n_p/n_e (panel f) also increases during this period.
The EMIC theoretical instability threshold and the observational growth parameter are
shown in panels g and h, respectively. There is a significant enhancement in the
observational growth parameter (peak value of $\Sigma_h = 0.26$) during the EMIC wave
activity. The final panel (i) marks the $\Sigma_h - S_h$ calculation, with a blue horizontal line
marking $\Sigma_h - S_h = 0$. Since $\Sigma_h - S_h > 0$, linear theory states that the observed plasma
conditions are favorable for EMIC wave excitation. Another $\Sigma_h - S_h > 0$ appears later in
the orbit, 1833 – 1837 UT, however no EMIC wave activity is observed during this
period. After applying linear theory to all observed events, 232 EMIC wave events (103
$\mathrm{H^{+}}$ -band and 129 $\mathrm{He^{+}}$ -band) were found to have positive $\Sigma_{h}-S_{h}$ values. Few EMIC
wave events with excitation favorable plasma conditions below $L = 4$ were included.

3.2 Calculation results

As described in Section 2.4, convective wave growth rates were calculated for each H⁺- and He⁺-band EMIC wave event with a positive $\Sigma_h - S_h$ value. For each of these events, their instantaneous density, T_l , and anisotropy measurements of H⁺, He⁺,

324

325

326

327

328

329

330

331

332

333

334

335

336

337

338

339

340

341

342

343

344

345

346

and O⁺ ions were used. The calculated electron density (Zhelavskaya et al., 2016) was used to determine the location of an EMIC wave event with respect to the plasmasphere. By visual inspection, events determined to be found near the plasmasphere received the enlarged MLAT integrated path described in Section 2.4.

The following plots have combined measurements from both Van Allen Probes. Figure 2 shows the comparison between the calculated EMIC wave amplitudes based off the *in situ* plasma measurements from the HOPE instrument (a) and the observed *in situ* EMIC wave amplitudes obtained from the EMFISIS instrument and subsequent polarization analysis (b), for the H⁺-band EMIC waves in L vs. MLT bins. Each bin comprises 15 min of MLT per 0.5 L shell. The resolution was chosen to be consistent with previous studies (Saikin et al., 2015, 2016). L shell was determined by using the 2004 Tsyganenko and Sitnov magnetic field model (TS04D) (Tsyganenko and Sitnov, 2005). Each EMIC wave event was divided into 1 min UT intervals, and plotted into the respective bin based off the L and MLT value during that 1 min UT duration. The values within those bins were then averaged over the amount of time within that respective bin, White spaces represent regions where neither Van Allen Probes has magnetic field measurements. Grey spaces represent regions where the Van Allen Probes do have magnetic field measurements, but no EMIC wave activity is observed. The percent difference between the observed and calculated EMIC wave amplitudes are shown in Figure 2c.

Throughout all MLT sectors, the calculation produces H^+ -band EMIC waves with wave amplitudes of ~0.10 nT. In the midnight sector, (2200 < MLT \leq ~130), EMIC wave amplitudes around ~1.0 nT are produced. Peak wave amplitudes are produced in the

afternoon sector, (1600 $<$ MLT \le 1700), \sim 10.0 nT. The calculation, however, fails to
reproduce the wave amplitudes observed by the Van Allen Probes. H+-band EMIC waves
observed by the Van Allen Probes possess wave amplitudes between ~1.0 – 5.0 nT
throughout all MLT sectors between $L = 4 - 6$. The lowest H ⁺ -band wave amplitudes,
~0.1 – ~0.3 nT, are observed primarily around $L = ~6$ within 0615 < MLT < ~1930.

The calculation repeatedly produces H^+ -band EMIC wave amplitudes that are too low when compared to the observed wave amplitudes. Percent differences between the calculated and observed wave amplitudes for almost every bin consistently feature negative percentages ranging from 50.0 - 100.0%. For comparison, the previously described $\pm 5^{\circ}$ MLAT source region has been expanded to the $\pm 11^{\circ}$ MLAT described in *Loto'aniu et al.* (2005) for all EMIC waves, regardless of their observation with respect to the plasmapause. In the same format as Figure 2, Figure 3 shows this recalculation with the extended integrated MLAT path. As expected, the increased wave path does produce EMIC waves with higher wave amplitudes than the previous $\pm 5^{\circ}$ MLAT setting. However, in the region of $L = \sim 6$, the calculation now produces EMIC waves with wave amplitudes beyond the values that are observed by the Van Allen Probes (Figure 3c).

Figure 4 compares the calculated wave amplitudes results (a) with the observed wave amplitudes (b) for the He⁺-band EMIC wave events. Like the H⁺-band results, the calculated He⁺-band wave amplitudes are generally ~0.1 nT. The calculation does produce higher wave amplitudes in the afternoon and midnight MLT sectors, ~1.0 – 10.0 nT. However, the calculation does not reproduce the observed He⁺-band wave amplitudes consistently (Figure 4c). Percent differences between the calculated and observed EMIC wave amplitudes continue to be predominately negative throughout all MLTs. Some

midnight sector bins do show good agreement between the calculated and observed wave amplitudes, $2300 < \text{MLT} \le 100$ from L = 5 - 7. Conversely, some calcuation results produce wave amplitudes greater than the observations in the afternoon sector (i.e., positive percent differences), $1500 < \text{MLT} \le 1700$ at $L = \sim 5.5$. Like Figure 3, the $\pm 11^{\circ}$ MLAT *Loto'aniu et al.* (2005) region was applied to the He⁺-band waves in Figure 5. Again, the calculation now produces EMIC wave amplitudes too high to match the observed amplitudes, specifically around $L = \sim 6$, and the midnight MLT sector (2200 < MLT ≤ 200).

Using the original $\pm 5^{\circ}$ MLAT integrated wave path ($\pm 10^{\circ}$ for events observed near the plasmapause), the *in situ* plasma measurements obtained from the HOPE instrument do not possess enough "free energy" to reproduce the coinciding observed H⁺-and He⁺-band EMIC wave amplitudes. The expanded $\pm 11^{\circ}$ MLAT *Loto'aniu et al.* (2005) source amplification region produces EMIC wave amplitudes too high compared to wave observations.

3.3 Plasma recalculations: A_{hp}

To understand the discrepancy between the calculated and observed wave amplitudes for both H⁺- and He⁺-band events, we explore the differences in the plasma parameters when EMIC waves are and are not present. EMIC wave favorable plasma conditions can be observed without the presence of any EMIC wave activity (Figure 1h).

Figure 6 shows the observed A_{hp} (the instantaneous measured value, averaged per L vs. MLT bin) for all periods where $\Sigma_h - S_h > 0$ (Figure 6a), and for all periods where $\Sigma_h - S_h > 0$ that coincide with EMIC waves (Figure 6b). Wave-band separation has not been considered for Figure 6. For all $\Sigma_h - S_h > 0$ periods, A_{hp} is rarely observed to be

$L = \sim 4$.	
~ 0.62. Furthermore, almost all regions observed	to have $\Sigma_h - S_h > 0$ are located beyond
The dusk and pre-midnight MLT sectors (1600 <	$MLT \le 2400$) have measured A_{hp} values
observed in the dawn sector (0 < MLT \leq 1200), v	with peak values reaching $A_{hp} = \sim 1.00$.
lower than $A_{hp} = \sim 0.62$. A_{hp} does exhibit an MLT	dependence. The highest A_{hp} values are

 A_{hp} values decrease when EMIC waves are present (Figure 6b). Without EMIC waves, the dawn MLT sector measures hot proton anisotropies between $A_{hp} = \sim 0.81$ to 1.00. With EMIC waves present, some dawn MLT sector regions observe $A_{hp} = \sim 0.62$ (a 26.6% to 46.9% decrease). The dusk MLT sector measures lower anisotropies ($A_{hp} = \sim 0.25$ to 0.44, an 85.1% to 34.0% decrease). The midnight MLT sector (MLT = 2300 – 0100) is the only region where A_{hp} was found to increase with the presence of EMIC waves, $A_{hp} = \sim 1.00$.

Since A_{hp} is lowered in the presence of EMIC waves, using their *in situ* measurements will generally not reproduce the observed wave amplitudes. To produce calculated wave amplitudes that match the Van Allen Probes' observations, we must determine the initial ion anisotropies responsible for the EMIC wave excitation.

The following has been performed using the originally $\pm 5^{\circ}$ MLAT ($\pm 10^{\circ}$ MLAT for plasmapause events) framework. Using our routine to calculate EMIC wave amplitude, we have tested each ion's anisotropy to determine which ion's anisotropy has the greatest impact on EMIC wave growth. Each ion population's anisotropy values were altered, A_h* , individually between $0.00 \le A_h* \le 2.00$ (e.g., while A_{hp} was altered, the *in situ* measurement of A_{hhe} and A_{ho} were used). Table 1 shows the percentage of calculated wave-band specific EMIC wave events that are calculated to come within ± 0.1 nT of the

observed EMIC wave amplitude when only that hot ion's specific anisotropy is altered.
For both H ⁺ - and He ⁺ -band events, altering A_{hp} yields the highest agreement with the
observed wave amplitude with 75.5% and 73.4%, respectively. By exclusively altering
the hot helium anisotropy (A_{hhe}^*) , only 11.8% and 20.2% of the H ⁺ - and He ⁺ -band EMIC
waves, respectively, match the observed wave amplitudes. The hot oxygen anisotropy
(A_{ho}^*) has the least impact on the H ⁺ -band EMIC waves, 10.8%. As with the A_{hhe}^* , only
20.2% of the He ⁺ -band calculated EMIC waves could match the observation when only
A_{ho} is altered.

Altering A_{hp} yields the greatest success in reproducing observed EMIC wave amplitudes (75.5% and 73.4% for H⁺- and He⁺-band, respectively). For each event, we retroactively calculated A_{hp} that yields the best agreement with the data. These altered anisotropy values A_{hp}^{*} are compared against the *in situ* A_{hp} in Figure 7. Displayed in Figure 7 is the ratio between A_{hp}^{*} and the observed A_{hp} (or amplification factors) for both the H⁺-band (Figure 7a) and He⁺-band events (Figure 7b) in the same L vs. MLT format.

Generally, the H⁺-band EMIC wave events observed throughout all MLT sectors are found to require increased A_{hp} values, ranging from $1 < A_{hp}*/A_{hp} \le 4$. Peak amplification factors (~4) are observed in the pre-noon (900 < MLT \le 1000), afternoon, and pre-midnight (2000 < MLT \le 2200) MLT sectors. The pre-noon and afternoon regions correspond to peak occurrence rates for H⁺-band EMIC waves (Saikin et al., 2015).

He⁺-band EMIC wave events require similar altered A_{hp} values in the dawn sector, $1 < A_{hp}*/A_{hp} \le \sim 3$. However, post-noon/dusk (1330 < MLT ≤ 2230) sector He⁺-band events require amplification factors ~ 3 - ~ 4 times than the *in situ* measurements to

reproduce the observed wave amplitudes. Peak He⁺-band wave occurrence and wave power is observed in the afternoon sector (Saikin et al., 2015). These high amplification factors suggest that high-powered EMIC waves are more efficient at scattering ring current protons and further reduce A_{hp} .

4. Discussion

In this study, we compared wave amplitudes between calculated and Van Allen Probes' observed EMIC wave events between 1 November 2012 – 31 August 2014, a full MLT precession by Van Allen Probes. Calculated wave amplitudes were determined using the *in situ* HOPE instrument plasma measurements which coincided with EMIC wave activity. EMIC wave events were selected based on a criterion incorporating event duration (\geq 5 minutes in UT), wave power (\geq 0.01 nT²), and plasma conditions favorable for EMIC wave excitation ($\Sigma_h - S_h > 0$). This study serves as an extension on previous observation-based (e.g., Blum et al., 2009; Zhang et al., 2014; Allen et al., 2016) and simulation-based (e.g., Jordanova et al., 2001; Bortnik et al., 2007; Fu et al., 2016) studies focusing on EMIC wave excitation by combining both observations and simulations.

4.1 Linear theory Limitations

Due to their increased presence in the ring current, protons typically are the free energy providers for EMIC wave generation when they are injected into the inner magnetosphere and overlap with cold plasma populations. The linear theory proxy calculation only explicitly includes the plasma parameters associated with hot protons and neglects the presence of hot helium or hot oxygen ions. Only by proxy are the contributions from cold ions present in linear theory in the form of the electron density.

This proxy does not include specific ratios of cold H^+ , He^+ , or O^+ ions which impact EMIC wave growth, especially which wave-bands EMIC waves are excited (Jordanova et al., 2001; Kozyra et al., 1984). This possible missing "free energy" from the hot He^+ or hot O^+ ions, along with the lack of a proper cold plasma distribution per event, may have caused some \mathcal{E}_h values to not exceed S_h , thereby registering an event with a negative $\mathcal{E}_h - S_h$ value. The proxy derived from the linear theory proxy was used to identify EMIC wave events with plasma parameters more favorable for EMIC wave excitation. Without incorporating the impact of the hot He^+ and hot O^+ ions, other EMIC wave events may have been considered for this study. However, Table 1 reveals that A_{hp} has a greater impact on EMIC wave amplitude than the A_{hhe} or A_{ho} . Furthermore, the contribution from hot He^+ or hot O^+ ions may be limited due to their relative low ring current densities (Fu et al., 2016). The possibility remains that heavy ions may damp the waves or may lower the wave growth rate for other wave-band events. The hot ring current H^+ population remains the greatest provider of "free energy" for EMIC wave excitation.

As described in section 2.3, the linear theory proxy is derived assuming a bi-Maxwellian velocity distribution for both protons and electrons. The use of bi-Maxwellian velocity distributions have been examined over the years in relation to EMIC wave generation (Allen et al., 2016; Blum et al., 2009; Gary et al., 1994; Lin et al., 2014; Zhang et al., 2014). However, the use of bi-Maxwellian distributions is not required. Another study has explored using kappa distributions to describe the instability threshold for EMIC wave excitation (Xiao et al., 2007). While focusing on a kappa plasma, bi-Maxwellian velocity distributions were found to overestimate the maximum wave growth

(Xiao et al., 2007). If the observational growth parameter is overestimated, then our event list of EMIC waves believed to have favorable plasma conditions for EMIC wave generation would decrease. While we have not assumed a kappa distribution in this current study, we may examine this as an alternative in future work.

The linear theory proxy does reveal periods of favorable plasma conditions where no EMIC wave activity is observed. These favorable regions without EMIC waves have been explored in a recent study (Saikin et al., Local plasma conditions during EMIC wave events detected in the inner magnetosphere by the Van Allen Probes, submitted to the Journal of Geophysical Research: Space Physics, 2017). Of the 1,793.8 hours of Van Allen Probes' observations in which plasma favorable for EMIC wave generation is observed, only 271.8 hours coincide with EMIC wave activity. The occurrence rate of EMIC waves does increase with higher positive values of $\Sigma_h - S_h$. Most periods of $\Sigma_h - S_h > 0$ in which no EMIC waves are observed, generally, have very low $\Sigma_h - S_h$ values (i.e., $\Sigma_h - S_h = \sim 0.001 - 0.1$). Calculated wave amplitudes based off these non-EMIC waves observed plasma conditions have not been performed and are reserved for future work.

Linear theory does not consider wave propagation effects. The possibility exists that EMIC waves are generated in a different region and propagate to the location where they are observed by the Van Allen Probes. Using a Poynting vector analysis could confirm whether the observed EMIC wave activity is found to be bi-directionally propagating, which is characteristic of newly generated EMIC waves (Allen et al., 2013; Loto'aniu et al., 2005). However, this paper emphasizes the comparison between in situ plasma parameters and linear instability predictions. Bi-directionally propagating EMIC wave events

are not necessarily observed in regions where plasma conditions are currently favorable for EMIC wave excitation. Future work should examine the relationship between bidirectional EMIC waves, their associated plasma conditions, and how well the linear theory proxy predicts their observation.

4.2 Higher-energy Wave Free Energy Provider

The Van Allen Probes' Radiation Belt Storm Probes Ion Composition Experiment (RBSPICE) instrument is designed to collect measurements of keV particles. Energy channels vary per species (H⁺: 10–10,000 keV, He⁺: 25–10,000 keV, O⁺: 40–10,000 keV). However, previous studies which used linear theory have not incorporated energetic particles greater than 52 keV (Allen et al., 2016; Blum et al., 2009; Lin et al., 2014; Zhang et al., 2014). Using satellites at geosynchronous orbits, hot proton populations between 100 eV – 45 keV were used for linear theory in the work by Blum et al. (2009). Both Lin et al. (2014) and Allen et al. (2016) examined EMIC wave excitation with measurements from the Cluster mission. The ion COmposition Distribution Function (CODIF) instrument onboard Cluster observes ions (H⁺, He⁺, and O⁺) with an energy per charge range between 0.04 – 40 keV/e. Another linear theory case study on EMIC wave excitation performed with the Van Allen Probes only used measurements from the HOPE instrument (~1 eV – 52 keV for H⁺, He⁺, and O⁺) (Zhang et al., 2014).

There are some RBSPICE energy channels which overlap with the HOPE instrument. However, to remain consistent with previous work, measurements from RBSPICE have been not included in this current study. Incorporating energetic particles beyond the HOPE energy range (> 52 keV) could possibly supply some of the missing "free energy", -thereby increasing the wave amplitudes of the calculated EMIC waves.

Follow-up studies examining EMIC wave excitation with linear theory may wish to include the more energetic particles measured by RBSPICE. Using the higher energetic (> 52 keV) proton populations would increase the hot proton density and therefore the observational growth parameter. More events would be considered to coincide with plasma conditions favorable for EMIC wave excitation. Calculated EMIC wave amplitudes may better replicate their observed counterparts.

4.3 Calculated EMIC wave amplitudes and A_{hp} requirements

EMIC wave excitation requires populations of hot anisotropic ions to overlap with cold dense plasma. Previous studies report a significant increase in EMIC wave observation and wave power in the afternoon sector (Anderson et al., 1992; Halford et al., 2010; Meredith et al., 2014; Min et al., 2012; Paulson et al., 2016; Saikin et al., 2016, 2015). Plasmaspheric plumes are often attributed with supplying the cold dense plasma in the afternoon sector (Fraser and Nguyen, 2001; Saikin et al., 2015; Usanova et al., 2013). The calculation used in this study includes a wave growth enhancement factor when EMIC wave activity is believed to be near cold plasmaspheric ion populations.

Using the cold plasmaspheric enhancement factor (i.e., the extended source region given to EMIC wave events believed to be near the plasmapause), the *in situ* Van Allen Probes' plasma measurements, and the calculated electron density (Zhelavskaya et al., 2016), the calculation produces H⁺- and He⁺-band EMIC wave events (Figures 2a and 3a, respectively) with enhanced (~1.0 – 10.0 nT) wave amplitudes in the afternoon sector. While not accurate to the observed EMIC wave amplitudes, the routine is successful in favoring this region for enhanced EMIC wave growth. Previous simulation studies have

also reproduced the EMIC wave-enhanced afternoon sector (Jordanova et al., 2001; Kozyra et al., 1997).

The calculation also produces enhanced (~1.0 nT) EMIC wave amplitudes in the midnight sector (2200 < MLT ≤ 200) for both the H⁺- and He⁺-band EMIC wave events. Other simulations have shown increased wave growth rates with respect to geomagnetic storm phases (Jordanova et al., 2001, 2014). During geomagnetic storms or substorms, plasma sheet ions may be injected into the inner magnetosphere from the magnetotail (Bossen et al., 1976; Cornwall, 1965; Jordanova et al., 2001). This would supply the hot plasma necessary for EMIC wave generation. Statistical studies examining the relationship between inner magnetosphere EMIC wave observations and geomagnetic activity have been performed (Halford et al., 2010, 2016; Keika et al., 2013; Meredith et al., 2014; Saikin et al., 2016). During geomagnetic disturbances, these studies repeatedly show peak EMIC waves observations occur in the afternoon sector, with limited observations in the night side magnetosphere. Varying levels of geomagnetic activity was not found to increase EMIC wave amplitudes in the midnight sector (Meredith et al., 2014). Future work should explore the relationship between the linear theory proxy, geomagnetic activity, and EMIC wave observations.

Figure 6a shows the A_{hp} values of all periods with plasma conditions considered favorable for EMIC wave excitation. The dawn side (0 < MLT \leq 1200) inner magnetosphere is observed to have higher measurements of A_{hp} than the dusk side (1200 < MLT \leq 2400) inner magnetosphere, consistent with previous studies (Allen et al., 2016; Min et al., 2012). This observed A_{hp} MLT asymmetry may be a symptom of magnetospheric dynamics. For example, injections supply the ring current with fresh

particles from the plasma sheet. Curvature and gradient drifts cause high-energy ions to drift westward while low-energy ions drift eastward. As the energetic (keV) ions drift they are subject to loss processes such as charge exchange (Keika et al., 2006; Kistler et al., 1998; Noël, 1997) and pitch angle scattering from EMIC waves (Burch et al., 2002; Jordanova et al., 2001). The afternoon sector, where most EMIC wave observations occur (Anderson et al., 1992; Halford et al., 2010; Kasahara et al., 1992; Keika et al., 2013; Meredith et al., 2014; Min et al., 2012; Saikin et al., 2015), is the region where A_{hp} decreases due to scattering EMIC waves (Figure 6a). Saikin et al. (2015) showed that the dayside magnetosphere, overall, has consistent EMIC wave occurrence rates (between 13 -25%). The noon sector EMIC waves could continue to scatter energetic ions, further increasing A_{hp} . Ions not impacted by these loss mechanisms would continue to drift to the dawn sector. With the population of loss cone vulnerable particles decreasing, the remaining ions, which continue to drift, would represent a more anisotropic ion population. Simulations have been able to reproduce this MLT asymmetry in the ring current (Kozyra et al., 1997). This trend is not observed in the outer ($> 10~R_{\rm e}$) magnetosphere (Allen et al., 2016).

597 598

599

600

601

602

603

604

581

582

583

584

585

586

587

588

589

590

591

592

593

594

595

596

Despite relatively higher ($\geq \sim 0.62$) A_{hp} measurements, EMIC waves are still preferably observed in the afternoon sector than the dawn sector (Anderson et al., 1992; Halford et al., 2010; Min et al., 2012; Saikin et al., 2015). Plasmaspheric plumes, which increase convective growth rates, are not as prevalent in the dawn sector compared to the afternoon sector (Goldstein et al., 2014). Limited availability of these cold plasma populations may inhibit EMIC wave excitation and observations in dawn side magnetospheric regions.

Generally, A_{hp} values are found to be lower in the presence of EMIC waves (Figure 6b), implying that these *in situ* measurements are not necessarily the initial anisotropy responsible for wave generation. Since the *in situ* measurements are not necessarily the EMIC wave inciting conditions, expanding the $\pm 5^{\circ}$ MLAT integrated path to $\pm 11^{\circ}$ MLAT (the *Loto'aniu et al.* (2005) source region) with the observed A_{hp} values would not exclusively explain the calculation producing EMIC waves with wave amplitudes too low to match the observations. The relationship between initial EMIC wave excitation plasma conditions with variable integrated wave paths MLAT regions should be examined, and is reserved for future work.

Given the linear theory proxy framework (Blum et al., 2009; Gary et al., 1994; Zhang et al., 2014), EMIC waves observed during intervals where $\Sigma_h - S_h > 0$, plasma conditions favorable for EMIC wave excitation, are inferred to be within the EMIC wave source region. These EMIC wave favorable plasma conditions continue to supply the EMIC wave activity with "free energy", i.e., increasing the wave amplitudes. As EMIC waves continue to grow, they begin to stabilize the anisotropic hot proton distributions responsible for the wave excitation (Gary et al., 1994) until wave amplitude saturation is reached. Similar results have been found in simulating EMIC wave amplitude saturation (Bortnik et al., 2011). In Figure 1 of their study, Bortnik et al. (2011) model wave amplitude saturation over time while focusing on the growth, saturation, and decay phase of the wave, During the growth phase, as the wave amplitude increases, the hot protons' $T_{\perp}(T_{\parallel})$ decreases (increases) indicating that the anisotropy has decreased from the initial starting condition.

Throughout all MLTs, H ⁺ - and He ⁺ -band events require higher A_{hp} values to
reproduce the data. Except for the pre-noon (800 $<$ MLT \leq 1000), the afternoon (1500 $<$
MLT \leq 1800), and the post-dusk (2000 $<$ MLT \leq 2200) sectors, on average H $^+$ -band
events require A_{hp} values twice what is observed during the EMIC wave observation. The
previously mentioned exceptions require A_{hp} values between ~3 to ~4 times greater than
the measured A_{hp} . These exception regions correspond to locations within the inner
magnetosphere where peak H ⁺ -band EMIC wave occurrence is observed (Saikin et al.,
2015).

He⁺-band EMIC waves have the highest observed wave power in the afternoon sector within the inner magnetosphere (Meredith et al., 2014; Saikin et al., 2015). The afternoon sector coincides with the known EMIC enhanced region (Thorne, 2010). To produce EMIC waves with higher wave amplitudes, dusk side He⁺-band EMIC waves require higher hot proton anisotropy amplification factors, ~4, compared to the He⁺-band EMIC wave events observed in other MLT regions. Increasing A_{hp} to produce higher EMIC wave amplitudes is consistent with previous works (Bortnik et al., 2011; Fu et al., 2016). Future studies should consider this A_{hp} decrease when examining EMIC wave generation using their *in situ* plasma observations.

Neither Bortnik et al. (2011) nor Fu et al. (2016) incorporated the use of *in situ* plasma measurements in their simulation studies. Bortnik et al. (2011) varied their hot proton density and anisotropy inputs, while keeping the density of cool (~eVs) plasma constant (H⁺: 4.66 cm⁻¹, He⁺: 0.04 cm⁻¹). Increasing either parameter produced higher wave amplitudes. No cool O⁺ ions were considered for their simulations. For their study, Bortnik et al. (2011) compared their simulated wave amplitudes to observations from the

Charge Composition Explorer (CCE) spacecraft in the Active Magnetospheric Particle Tracer Explorers (AMPTE) mission. While focusing on the outer dawn and dayside magnetosphere (L ~ 9), AMPTE/CCE observed wave amplitudes between 1.6 nT - 2.5 nT, respectively (Anderson et al., 1992). Using their typical simulated saturation amplitudes, Bortnik et al. (2011) produced EMIC wave amplitudes between 0.4 nT – 2.6 nT, generally in good agreement with Anderson et al. (1992). AMPTE/CCE's orbit extends beyond the range of the Van Allen Probes' orbit and disproportionately favors outer magnetosphere EMIC wave measurements (Saikin et al., 2015). Despite these orbital differences, EMIC wave amplitudes remain similar for both the H⁺- and He⁺-band wave events (Figures 2b and 3b, respectively).

Fu et al. (2016) utilized their hybrid simulations with the linear theory proxy parameters (β_{lhp} , A_{hp} , and n_{hp}/n_e) to predict EMIC wave amplitudes. The impact of hot He⁺ ions was ignored due to their relatively low ring current density. Their simulations reveal that when the wave amplitude saturates, A_{hp} begins to decrease in response to EMIC waves scattering hot protons. Our results using the Van Allen Probes in situ measurements support this notion. The Van Allen Probes measure higher A_{hp} values when EMIC waves events are not observed. Fu et al. (2016) further expands on their simulations by deriving an equation for wave amplitude saturation as a function of β_{lhp} , n_{hp}/n_e , and n_{he}/n_e . No specifications are made within Fu et al. (2016) with respect to magnetospheric location, only the magnetic field magnitude, nor if there exists an A_{hp} MLT asymmetry.

5. Conclusion

In this paper, we have calculated EMIC wave amplitudes based off in situ plasma
measurements from the Van Allen Probes' HOPE instrument. These calculated wave
amplitudes were compared with EMIC wave events associated with those plasma
conditions. This analysis focused on EMIC waves observed during plasma conditions
considered favorable for EMIC wave generation. The study examines events between 1
November 2012 and 31 August 2014, a full MLT precession for the Van Allen Probes.
Two hundred and thirty-two EMIC wave observations (103 H ⁺ -band and 129 He ⁺ -band)
were found to coincide with favorable plasma conditions for EMIC wave excitation. The
results based on comparing the calculated and observed EMIC wave amplitudes can be
summarized as such:

1.) Using exclusively *in situ* plasma measurements, the calculations cannot reproduce the observed wave amplitudes for either H^+ - or He^+ -band EMIC wave events. Often the calculated events require more "free energy" than the *in situ* measurements yield. The calculation does produce wave amplitude enhancements in the afternoon (1500 < MLT \leq 1700) sector consistent with previously observed results (e.g., Meredith et al., 2014; Saikin et al., 2015).

2.) A_{hp} distributions in the inner (L < 7) magnetosphere are asymmetric in MLT. In the dawn (dusk), $0000 < \text{MLT} \le 1200$ ($1200 < \text{MLT} \le 2400$), sector A_{hp} are measured between 0.81 - 1.00 (~ 0.62). A_{hp} generally decreases when EMIC waves are present.

3.) The anisotropy of hot ($\geq 1 \text{ keV}$) H⁺ has a greater impact on EMIC wave saturation amplitudes than the anisotropies of hot He⁺ or hot O⁺. Varying values of A_{hp} could

696	replicate observed EMIC wave amplitudes for ~75.5 % (73.4%) of the H ⁺ -band
697	(He ⁺ -band) events. Altering A_{hhe} or A_{ho} only replicated ~10.8% - ~20.2% of the
698	observed wave amplitudes.
699	4.) The required A_{hp} to reproduce EMIC wave events varies with wave-band and
700	MLT. H ⁺ -band events (He ⁺ -band), generally, require double the <i>in situ</i> measured
701	A_{hp} throughout all MLTs (0000 < MLT \leq 1200). Dusk (1200 < MLT \leq 2400)
702	sector: He^+ -band events require quadruple the <i>in situ</i> measured A_{hp} to reproduce
703	their observed wave amplitudes.
704	
705	
706	
707	
708	
709	
710	
711	
712	
713	
714	
715	
716	
717	
718	
719	
720	

Acknowledgments:
This work was supported by the Los Alamos Space Weather Summer School, funded by the Center for Space and Earth Sciences at Los Alamos National Laboratory. Work at UNH was supported by NASA under grant numbers NNX11AO82G and NNX15AF66G. This work was also supported by Iowa subcontract 1000556126 to UNH in support of the Van Allen Probes and EMFISIS/MAG instruments and by RBSP-ECT funding provided by JHU/APL contract 967399 under NASA's Prime contract NAS5-01072. Work at the University of Iowa was performed under support on JHU/APL contract 921647 under NASA's Prime contract NAS501072. Work at Los Alamos is performed under the auspices of the US Department of Energy, through contract DE-AC52-06NA25396. The authors thank Van Allen Probes team members for Van Allen Probes data preparation. A. A. Saikin thanks Lynn Kistler, Eric Lund, and Christopher Mouikis for helpful discussion. Special thanks are also given to Robert Allen for help in developing software routines. The data used in this study were obtained from the EMFISIS data directory at http://emfisis.physics.uiowa.edu, and the ECT data directory at https://www.rbsp-ect.lanl.gov.php.

756	
757	
758	
759	
760	References
761	
762 763 764 765	Allen, R.C., Zhang, JC., Kistler, L.M., Spence, H.E., Lin, R.L., Dunlop, M.W., André, M., 2013. Multiple bidirectional EMIC waves observed by Cluster at middle magnetic latitudes in the dayside magnetosphere. J. Geophys. Res. Sp. Phys. 118, 6266–6278. doi:10.1002/jgra.50600
766 767 768 769	Allen, R.C., Zhang, JC., Kistler, L.M., Spence, H.E., Lin, RL., Klecker, B., Dunlop, M.W., Andre, M., Jordanova, V.K., 2016. A statistical study of EMIC waves observed by Cluster: 2. Associated plasma conditions. J. Geophys. Res. Sp. Phys. 121, 6458–6479. doi:10.1002/2016JA022382.Received
770 771 772 773	Allen, R.C., Zhang, JC., Kistler, L.M., Spence, H.E., Lin, RL., Klecker, B., Dunlop, M.W., André, M., Jordanova, V.K., 2015. A statistical study of EMIC waves observed by Cluster: 1. Wave properties. J. Geophys. Res. Sp. Phys. 120, 5574–5592. doi:10.1002/2015JA021333
774 775 776	Anderson, B.J., Erlandson, R.E., Zanetti, L.J., 1992. A statistical study of Pc 1-2 magnetic pulsations in the equatorial magnetosphere I. Equatorial occurrence distributions. J. Geophys. Res. 97, 3075–3088. doi:10.1029/91JA02706
777 778 779	Anderson, B.J., Hamilton, D.C., 1993. Electromagnetic ion cyclotron waves stimulated by modest magnetospheric compressions. J. Geophys. Res. 98, 11369–11383. doi:10.1029/93JA00605
780 781 782	Blum, L.W., MacDonald, E.A., Gary, S.P., Thomsen, M.F., Spence, H.E., 2009. Ion observations from geosynchronous orbit as a proxy for ion cyclotron wave growth during storm times. J. Geophys. Res. 114, A10214–A10223. doi:10.1029/2009JA014396
783 784 785	Bortnik, J., Cutler, J.W., Dunson, C., Bleier, T.E., 2007. An automatic wave detection algorithm applied to Pc1 pulsations. J. Geophys. Res. Sp. Phys. 112, A04204–A04216. doi:10.1029/2006JA011900
786 787 788	Bortnik, J., Omidi, N., Chen, L., Thorne, R.M., Horne, R.B., 2011. Saturation characteristics of electromagnetic ion cyclotron waves. J. Geophys. Res. Sp. Phys. 116, 1–10. doi:10.1029/2011JA016638
789 790	Bossen, M., Mcpherron, R.L., Russell, C.T., 1976. A statistical study of Pc 1 magnetic pulsations at synchronous orbit. J. Geophys 81, 6083–6091.
791 792	Burch, J.L., Lewis, W.S., Immel, T.J., Anderson, P.C., Frey, H.U., Fuselier, S.A., G??rard, J.C., Mende, S.B., Mitchell, D.G., Thomsen, M.F., 2002, Interplanetary magnetic field control of

- afternoon-sector detached proton auroral arcs. J. Geophys. Res. Sp. Phys. 107, 1–13.
- 794 doi:10.1029/2001JA007554
- 795 Cornwall, J.M., 1965. Cyclotron instabilities and electromagnetic emission in the ultra low
- frequency and very low frequency ranges. J. Geophys. Res. 70, 61–69.
- 797 doi:10.1029/JZ070i001p00061
- Criswell, D.R., 1969. Pc 1 micropulsation activity and magnetospheric amplification of 0.2- to
- 5.0-Hz hydromagnetic waves. J. Geophys. Res. Sp. Phys. 74, 205–224.
- doi:10.1029/JA074i001p00205
- Denton, R.E., Jordanova, V.K., Fraser, B.J., 2014. Effect of spatial density variation and O +
- concentration on the growth and evolution of electromagnetic ion cyclotron waves. J.
- 803 Geophys. Res. 119, 8372–8395. doi:10.1002/2014JA020384.Received
- 804 Engebretson, M.J., Yeoman, T.K., Oksavik, K., Søraas, F., Sigernes, F., Moen, J.I., Johnsen,
- M.G., Pilipenko, V. a., Posch, J.L., Lessard, M.R., Lavraud, B., Hartinger, M.D., Clausen,
- L.B.N., Raita, T., Stolle, C., 2013. Multi-instrument observations from Svalbard of a
- traveling convection vortex, electromagnetic ion cyclotron wave burst, and proton
- precipitation associated with a bow shock instability. J. Geophys. Res. Sp. Phys. 118, 2975–
- 809 2997. doi:10.1002/jgra.50291
- 810 Fraser, B.J., Grew, R.S., Morley, S.K., Green, J.C., Singer, H.J., Loto'aniu, T.M., Thomsen,
- M.F., 2010. Storm time observations of electromagnetic ion cyclotron waves at
- geosynchronous orbit: GOES results. J. Geophys. Res. 115, A05208–A05223.
- 813 doi:10.1029/2009JA014516
- Fraser, B.J., Kemp, W.J., Webster, D.J., 1989. Ground-satellite study of a Pc 1 ion cyclotron
- wave event. J. Geophys. Res. 94, 11855–11863.
- Fraser, B.J., Nguyen, T.S., 2001. Is the plasmapause a preferred source region of electromagnetic
- ion cyclotron waves in the magnetosphere? J. Atmos. Solar-Terrestrial Phys. 63, 1225–
- 818 1247. doi:10.1016/S1364-6826(00)00225-X
- 819 Fu, X., Cowee, M.M., Jordanova, V.K., Gary, S.P., Reeves, G.D., Winske, D., 2016. Predicting
- 820 electromagnetic ion cyclotron wave amplitude from unstable ring current plasma
- 821 conditions. J. Geophys. Res. Sp. Phys. 121, 1–12. doi:10.1002/2016JA023303
- Funsten, H.O., Skoug, R.M., Guthrie, A.A., MacDonald, E.A., Baldonado, J.R., Harper, R.W.,
- Henderson, K.C., Kihara, K.H., Lake, J.E., Larsen, B.A., Puckett, A.D., Vigil, V.J., Friedel,
- R.H., Henderson, M.G., Niehof, J.T., Reeves, G.D., Thomsen, M.F., Hanley, J.J., George,
- D.E., Jahn, J.M., Cortinas, S., De Los Santos, A., Dunn, G., Edlund, E., Ferris, M.,
- Freeman, M., Maple, M., Nunez, C., Taylor, T., Toczynski, W., Urdiales, C., Spence, H.E.,
- Cravens, J.A., Suther, L.L., Chen, J., 2013. Helium, oxygen, proton, and electron (HOPE)
- mass spectrometer for the Radiation Belt Storm Probes mission. Sp. Sci Rev 423–484.
- doi:10.1007/978-1-4899-7433-4-13
- 830 Gamayunov, K. V, Engebretson, M.J., Zhang, M., Rassoul, H.K., 2014. Model of
- electromagnetic ion cyclotron waves in the inner magnetosphere. J. Geophys. Res. 119,
- 832 7541–7565. doi:10.1002/2014JA020032.Received

- Gary, S.P., Moldwin, M.B., Thomsen, M.F., Winske, D., McComas, D.J., 1994. Hot proton
- anisotropies and cool proton temperatures in the outer magnetosphere. J. Geophys. Res. Sp.
- Phys. 99, 23603–23615. doi:10.1029/94JA02069
- 636 Goldstein, J., Thomsen, M.F., Dejong, A., 2014. In situ signatures of residual plasmaspheric
- plumes: Observations and simulation. J. Geophys. Res. Sp. Phys. 119, 4706–4722.
- 838 doi:10.1002/2014JA019953.Received
- Halford, A.J., Fraser, B.J., Morley, S.K., 2010. EMIC wave activity during geomagnetic storm
- and nonstorm periods: CRRES results. J. Geophys. Res. Sp. Phys. 115, A12248–A12263.
- 841 doi:10.1029/2010JA015716
- Halford, A.J., Fraser, B.J., Morley, S.K., Elkington, S.R., Chan, A.A., 2016. Dependence of
- EMIC wave parameters during quiet, geomagnetic storm, and geomagnetic storm phase
- times. J. Geophys. Res. A Sp. Phys. 6277–6291. doi:10.1002/2016JA022694
- Horne, R.B., Thorne, R.M., 1993. On the preferred source location for the convective
- amplification of ion cyclotron waves. J. Geophys. Res. 98, 9233–9247.
- 847 doi:10.1029/92JA02972
- Jordanova, V.K., Albert, J., Miyoshi, Y., 2008. Relativistic electron precipitation by EMIC
- waves from self-consistent global simulations. J. Geophys. Res. Sp. Phys. 113, A00A10-
- 850 A00A21. doi:10.1029/2008JA013239
- Jordanova, V.K., Farrugia, C.J., Thorne, R.M., Khazanov, G. V., Reeves, G.D., Thomsen, M.F.,
- 852 2001. Modeling ring current proton precipitation by electromagnetic ion cyclotron waves
- during the May 14–16, 1997, storm. J. Geophys. Res. 106, 7–22.
- 854 doi:10.1029/2000JA002008
- Jordanova, V.K., Spasojevic, M., Thomsen, M.F., 2007. Modeling the electromagnetic ion
- cyclotron wave-induced formation of detached subauroral proton arcs. J. Geophys. Res. Sp.
- Phys. 112, A08209–A08222. doi:10.1029/2006JA012215
- Jordanova, V.K., Yu, Y., Niehof, J.T., Skoug, R.M., Reeves, G.D., Kletzing, C.A., Fennell, J.F.,
- Spence, H.E., 2014. Simulations of inner magnetosphere dynamics with an expanded RAM-
- SCB model and comparisons with Van Allen Probes observations. Geophys. Res. Lett. 41,
- 861 2687–2694. doi:10.1002/2014GL059533
- Kasahara, Y., Sawada, A., Yamamoto, M., Kimura, I., Kokubun, S., Hayashi, K., 1992. Ion
- cyclotron emissions observed by the satellite Akebono in the vicinity of the magnetic
- 864 equator. Radio Sci. 27, 347–362.
- Keika, K., Nosé, M., Brandt, P.C., Ohtani, S., Mitchell, D.G., Roelof, E.C., 2006. Contribution
- of charge exchange loss to the storm time ring current decay: IMAGE/HENA observations.
- J. Geophys. Res. Sp. Phys. 111, 1–13. doi:10.1029/2006JA011789
- Keika, K., Takahashi, K., Ukhorskiy, A.Y., Miyoshi, Y., 2013. Global characteristics of
- 869 electromagnetic ion cyclotron waves: Occurrence rate and its storm dependence. J.
- Geophys. Res. Sp. Phys. 118, 4135–4150. doi:10.1002/jgra.50385
- Kennel, C.F., Petschek, H.E., 1966. Limits on stably trapped particle fluxes. J. Geophys. Res. 71,
- 872 1–28. doi:10.1177/1069072705283987

- Kessel, R.L., Fox, N.J., Weiss, M., 2013. The Radiation Belt Storm Probes (RBSP) and Space
 Weather. Space Sci. Rev. 179, 531–543. doi:10.1007/s11214-012-9953-6
- Khazanov, G. V., Gamayunov, K. V., 2007. Effect of electromagnetic ion cyclotron wave normal angle distribution on relativistic electron scattering in outer radiation belt. J. Geophys. Res. Sp. Phys. 112, 1–9. doi:10.1029/2007JA012282
- 8// Sp. Phys. 112, 1–9. doi:10.1029/200/JA012282
- Kistler, L.M., Mobius, E., Klumpar, D.M., Popecki, M.A., Tang, L., Jordanova, V., Klecker, B.,
 Peterson, W.K., Shelley, E.G., Hovestadt, D., Carlson, C.W., Mozer, F.S., Strangeway, R.J.,
 Cattell, C.A., F, R., 1998. FAST/TEAMS observations of charge exchange signatures in
- ions mirroring at low altitudes. Geophys. Res. Lett. 25, 2085–2088.
- Kletzing, C.A., Kurth, W.S., Acuna, M., MacDowall, R.J., Torbert, R.B., Averkamp, T., Bodet,
- D., Bounds, S.R., Chutter, M., Connerney, J., Crawford, D., Dolan, J.S., Dvorsky, R.,
- Hospodarsky, G.B., Howard, J., Jordanova, V., Johnson, R. a., Kirchner, D.L., Mokrzycki,
- B., Needell, G., Odom, J., Mark, D., Pfaff, R., Phillips, J.R., Piker, C.W., Remington, S.L.,
- Rowland, D., Santolik, O., Schnurr, R., Sheppard, D., Smith, C.W., Thorne, R.M., Tyler, J.,
- 2013. The Electric and Magnetic Field Instrument Suite and Integrated Science (EMFISIS)
- on RBSP. Space Sci. Rev. 179, 127–181. doi:10.1007/s11214-013-9993-6
- Kozyra, J.U., Cravens, T.E., Nagy, A.F., Fontheim, E.G., 1984. Effects of energetic heavy ions
 on electromagnetic ion cyclotron wave generation in the plasmapause region. J. Geophys.
 Res. 89, 2217–2233.
- Kozyra, J.U., Jordanova, V.K., Home, R.B., Thorne, R.M., Horne, R.B., 1997. Modeling of the contribution of electromagnetic ion cyclotron (EMIC) waves to stormtime ring current erosion. Magn. Storms 98, 187–202. doi:10.1029/GM098p0187
- Lin, R.-L., Zhang, J.-C., Allen, R.C., Kistler, L.M., Mouikis, C.G., Gong, J.-C., Liu, S.-Q., Shi,
 L.-Q., Klecker, B., Sauvaud, J.-A., Dunlop, M.W., 2014. Testing linear theory of EMIC
 waves in the inner magnetosphere: Cluster observations. J. Geophys. Res. Sp. Phys. 119,
 1004–1027. doi:10.1002/2013JA019541
- Lockwood, M., Cowley, S.W.H., Sandholt, P.E., Lepping, R.P., 1990. The ionospheric
 signatures of flux transfer events and solar wind dynamic pressure changes. J. Geophys.
 Res. 95, 17113–17135. doi:10.1029/JA095iA10p17113;
- Loto'aniu, T.M., Fraser, B.J., Waters, C.L., 2005. Propagation of electromagnetic ion cyclotron
 wave energy in the magnetosphere. J. Geophys. Res. Sp. Phys. 110, A07214–A07224.
 doi:10.1029/2004JA010816
- Lyons, L.R., Thorne, R.M., Kennel, C.F., 1972. Pitch-Angle diffusion of radiation belt electrons
 within the plasmasphere. J. Atmos. Solar-Terrestrial Phys. 77, 3455–3474.
 doi:10.1029/JA077i028p05608
- Mauk, B.H., Fox, N.J., Kanekal, S.G., Kessel, R.L., Sibeck, D.G., Ukhorskiy, A., 2013. Science
 objectives and rationale for the radiation belt storm probes mission. Space Sci. Rev. 179, 3–
 doi:10.1007/s11214-012-9908-y
- 911 Mauk, B.H., McPherron, R.L., 1980. An experimental test of the electromagnetic ion cyclotron instability within the earth's magnetosphere. Phys. Fluids 23, 2111–2127.

913	doi:10.1063/1.862873
914 915 916	McCollough, J.P., Elkington, S.R., Baker, D.N., 2012. The role of Shabansky orbits in compression-related electromagnetic ion cyclotron wave growth. J. Geophys. Res. 117, A01208–A01220. doi:10.1029/2011JA016948
917 918 919	Meredith, N.P., Horne, R.B., Kersten, T., Fraser, B.J., Grew, R.S., 2014. Global morphology and spectral properties of EMIC waves derived from CRRES observations. J. Geophys. Res. 119, 5328–5342. doi:10.1002/2014JA020064
920 921 922 923	Meredith, N.P., Thorne, R.M., Horne, R.B., Summers, D., Fraser, B.J., Anderson, R.R., 2003. Statistical analysis of relativistic electron energies for cyclotron resonance with EMIC waves observed on CRRES. J. Geophys. Res. Sp. Phys. 108, A6–A20. doi:10.1029/2002JA009700
924 925	Min, K., Lee, J., Keika, K., Li, W., 2012. Global distribution of EMIC waves derived from THEMIS observations. J. Geophys. Res. 117, 1–13. doi:10.1029/2012JA017515
926 927	Morley, S.K., Ables, S.T., Sciffer, M.D., Fraser, B.J., 2009. Multipoint observations of Pc1-2 waves in the afternoon sector. J. Geophys. Res. 114, 1–14. doi:10.1029/2009JA014162
928 929	Noël, S., 1997. Decay of the magnetospheric ring current: A Monte Carlo simulation. J. Geophys. Res. 102, 2301. doi:10.1029/96JA03275
930 931	Omidi, N., Thorne, R., Bortnik, J., 2011. Hybrid simulations of EMIC waves in a dipolar magnetic field. J. Geophys. Res. Sp. Phys. 116, 1–16. doi:10.1029/2011JA016511
932 933 934	Paulson, K.W., Smith, C.W., Lessard, M.R., Torbert, R.B., Kletzing, C.A., Wygant, J.R., 2016. In Situ Statistical Observations of Structured and Unstructured EMIC Waves by the Van Allen Probes. J. Geophys. Res. Sp. Phys. doi:10.1002/2016JA023160
935 936 937	Rauch, J.L., Roux, A., 1982. Ray tracing of ULF waves in a multicomponent magnetospheric plasma: Consequences for the generation mechanism of ion cyclotron waves. J. Geophys. Res. 87, 8191–8198. doi:10.1029/JA087iA10p08191
938 939 940	Roux, A., Perraut, S., Rauch, J.L., De Villedary, C., Kremser, G., Korth, A., Young, D.T., 1982. Wave-particle interactions near ΩHe+ observed on board GEOS 1 and 2 2. Generation of ion cycltron waves and heating of He+ ions. J. Geophys. Res. 87, 8174–8190.
941 942 943 944	Saikin, A.A., Zhang, JC., Allen, R.C., Smith, C.W., Kistler, L.M., Spence, H.E., Torbert, R.B., Kletzing, C.A., Jordanova, V.K., 2015. The occurrence and wave properties of H+-, He+-, and O+-band EMIC waves observed by the Van Allen Probes. J. Geophys. Res. Sp. Phys. 120, 1–16. doi:10.1002/2015JA021358.
945 946 947 948	Saikin, A.A., Zhang, JC., Smith, C.W., Spence, H.E., Torbert, R.B., Kletzing, C.A., 2016. The dependence on geomagnetic conditions and solar wind dynamic pressure of the spatial distributions of EMIC waves observed by the Van Allen Probes. J. Geophys. Res. Sp. Phys. 121, 4362–4377. doi:10.1002/2016JA022606

Sakaguchi, K., Shiokawa, K., Miyoshi, Y., Otsuka, Y., Ogawa, T., Asamura, K., Connors, M.,

subauroral latitudes. J. Geophys. Res. 113, 1–12. doi:10.1029/2007JA012888

2008. Simultaneous appearance of isolated auroral arcs and Pc 1 geomagnetic pulsations at

949

950

- Shabansky, V.P., 1971. Some processes in the magnetosphere. Space Sci. Rev. 12, 299–418.
 doi:10.1007/BF00165511
- 954 Spence, H.E., Reeves, G.D., Baker, D.N., Blake, J.B., Bolton, M., Bourdarie, S., Chan, A.A.,
- 955 Claudepierre, S.G., Clemmons, J.H., Cravens, J.P., Elkington, S.R., Fennell, J.F., Friedel,
- 956 R.H.W., Funsten, H.O., Goldstein, J., Green, J.C., Guthrie, A., Henderson, M.G., Horne,
- 957 R.B., Hudson, M.K., Jahn, J.M., Jordanova, V.K., Kanekal, S.G., Klatt, B.W., Larsen, B.A.,
- Li, X., MacDonald, E.A., Mann, I.R., Niehof, J., O'Brien, T.P., Onsager, T.G., Salvaggio,
- D., Skoug, R.M., Smith, S.S., Suther, L.L., Thomsen, M.F., Thorne, R.M., 2013. Science
- goals and overview of the Radiation Belt Storm Probes (RBSP) Energetic Particle,
- Composition, and Thermal Plasma (ECT) suite on NASA's Van Allen Probes mission. Sp.
- 962 Sci Rev 311–336. doi:10.1007/978-1-4899-7433-4-10
- Thorne, R.M., 2010. Radiation belt dynamics: The importance of wave-particle interactions.
- 964 Geophys. Res. Lett. 37, 1–7. doi:10.1029/2010GL044990
- Thorne, R.M., Horne, R.B., 1997. Modulation of electromagnetic ion cyclotron instability due to
- interaction with ring current O+ during magnetic storms. J. Geophys. Res. 102, 14155–
- 967 14163. doi:10.1029/96JA04019
- Thorne, R.M., Kennel, C.F., 1971. Relativistic electron precipitation during magnetic storm main phase. J. Geophys. Res. 76, 4446–4453.
- 970 Tsyganenko, N.A., Sitnov, M.I., 2005. Modeling the dynamics of the inner magnetosphere 971 during strong geomagnetic storms. J. Geophys. Res. 110, 1–16. doi:10.1029/2004JA010798
- Usanova, M.E., Darrouzet, F., Mann, I.R., Bortnik, J., 2013. Statistical analysis of EMIC waves
- in plasmaspheric plumes from Cluster observations. J. Geophys. Res. 118, 4946–4951.
- 974 doi:10.1002/jgra.50464
- Usanova, M.E., Mann, I.R., Bortnik, J., Shao, L., Angelopoulos, V., 2012. THEMIS observations
- of electromagnetic ion cyclotron wave occurrence: Dependence on AE, SYMH, and solar
- 977 wind dynamic pressure. J. Geophys. Res. 117, 1–13. doi:10.1029/2012JA018049
- 978 Usanova, M.E., Mann, I.R., Kale, Z.C., Rae, I.J., Sydora, R.D., Sandanger, M., Søraas, F.,
- Glassmeier, K.-H., Fornacon, K.-H., Matsui, H., Puhl-Quinn, P.A., Masson, A., Vallières,
- 980 X., 2010. Conjugate ground and multisatellite observations of compression-related EMIC
- 981 Pc1 waves and associated proton precipitation. J. Geophys. Res. Sp. Phys. 115.
- 982 doi:10.1029/2009JA014935
- Wang, D., Yuan, Z., Yu, X., Deng, X., Zhou, M., Huang, S., Li, H., Wang, Z., Kletzing, C.A.,
- Wygant, J.R., 2015. Statistical characteristics of EMIC waves: Van Allen Probe
- 985 observations. J. Geophys. Res. Sp. Phys. 120, 6199–6206.
- 986 doi:10.1002/2015JA021354.Received
- 987 Xiao, F., Chen, L., He, Y., Su, Z., Zheng, H., 2011. Modeling for precipitation loss of ring
- 988 current protons by electromagnetic ion cyclotron waves. J. Atmos. Solar-Terrestrial Phys.
- 989 73, 106–111. doi:10.1016/j.jastp.2010.01.007
- Xiao, F., Yang, C., Zhou, Q., He, Z., He, Y., Zhou, X., Tang, L., 2012. Nonstorm time scattering
- of ring current protons by electromagnetic ion cyclotron waves. J. Geophys. Res. Sp. Phys.

992	117, 1–8. doi:10.1029/2012JA017922			
993 994 995	Xiao, F., Zhou, Q., He, H., Zheng, H., Wang, S., 2007. Electromagnetic ion cyclotron waves instability threshold condition of suprathermal protons by kappa distribution. J. Geophys. Res. Sp. Phys. 112, 1–8. doi:10.1029/2006JA012050			
996 997	Xiao, F., Zong, Q., Su, Z., Yang, C., He, Z., Wang, Y., Gao, Z., 2013. Determining the mechanism of cusp proton aurora. Sci. Rep. 3. doi:10.1038/srep01654			
998 999 1000 1001 1002	D., 1981. Wave-Particle Interactions Near Observed on GEOS 1 and 2 of Ion Cyclotron Waves in He + -Rich Plasma Max-Planck-Institut far Katlenburg-Lindau 3, made with ESA / GEOS 1 and 2 spacecraft which give an purpose. J. Geophys. Res. 86, 6755–6772			
1003 1004 1005	Yu, X., Yuan, Z., Wang, D., Li, H., Huang, S., Wang, Z., Zheng, Q., Zhou, M., Kletzing, C. a., Wygant, J.R., 2015. In situ observations of EMIC waves in O + band by the Van Allen Probe A. Geophys. Res. Lett. doi:10.1002/2015GL063250			
1006 1007 1008	Zhang, JC., Kistler, L.M., Mouikis, C.G., Dunlop, M.W., Klecker, B., Sauvaud, JA., 2010. A case study of EMIC wave-associated He+ energization in the outer magnetosphere: Cluster and Double Star 1 observations. J. Geophys. Res. 115, 1–17. doi:10.1029/2009JA014784			
1009 1010 1011	statistical study of EMIC wave-associated He+ energization in the outer magnetosphere:			
1012 1013 1014 1015	Zhang, JC., Saikin, A.A., Kistler, L.M., Smith, C.W., Spence, H.E., Mouikis, C.G., Torbert, R.B., Larsen, B.A., Reeves, G.D., Skoug, R.M., Funsten, H.O., Kurth, W.S., Kletzing, C.A. Allen, R.C., Jordanova, V.K., 2014. Excitation of EMIC waves detected by the Van Allen Probes on 28 April 2013. Geophys. Res. Lett. 41, 4101–4108. doi:10.1002/2014GL060621			
1016 1017 1018	Zhelavskaya, I.S., Spasojevic, M., Shprits, Y.Y., Kurth, W.S., 2016. Automated determination of electron density from electric field measurements on the Van Allen Probes spacecraft. J. Geophys. Res. A Sp. Phys. 121, 4611–4625. doi:10.1002/2015JA022132			
1019				
1020				
1021				
1022				
1023				
1024				
1025				
1026				
1027				

1028	
1029	
1030	
1031	
1032	
1033	
1034	
1035	
1036	
1037	
1038	
1039	
1040	
1041	
1042	
1043	
1044	Captions:
1045	Figure 1. Sample EMIC wave event and linear theory analysis
1046 1047 1048 1049 1050 1051 1052 1053	Caption: A He ⁺ -band EMIC wave event (a) observed between $1705 - 1715$ UT on 25 May 2013 and its corresponding linear theory analysis. Wave power (in nT ² /Hz) less than the 0.01 nT ² /Hz threshold has been marked white. Greed dashed lines mark the start (1705 UT) and end (1715 UT) times of the sample EMIC wave event, with solid green lines mapping them to the linear theory parameters. Figures b-i showcase the hot proton anisotropy (A_{hp}), the parallel hot proton β (β_{llhp}), the hot (≥ 1 keV) proton density (n_{hp}), the electron density (n_e), the ratio of n_{hp} and n_e , the theoretical EMIC instability (S_h), the observational growth parameter (?? $_h$), and ?? $_h - S_h$, respectively. The translucent green box marks the duration of the EMIC wave activity. A blue horizontal line has been over-plotted on panel h to mark ?? $_h - S_h = 0$.
1055	
1056 1057	Figure 2. Comparison between calculated and observed H+-band EMIC wave amplitudes $(\pm 5^\circ/\pm 10^\circ$ MLAT source region)
1058 1059 1060	Figure 2. The wave amplitudes of H ⁺ -band EMIC waves as calculated by the calculation (a), the wave amplitudes observed by the Van Allen Probes (b), and the relative difference between the simulation and observation (c). Each cell refers to 15 min in MLT per half L shell. Over-plotted

1061 1062	on this plot are circles representing the L =2, 4, 6, and 8 shells, respectively. Grey areas refer to the regions where the Van Allen Probes were located but did not observe EMIC wave activity.				
1063					
1064 1065	Figure 3. Comparison between calculated and observed \mathbf{H}^+ -band EMIC wave amplitudes (± 11 MLAT source region)				
1066 1067	Figure 3. Same format as Figure 2 but showing the analysis for the H^+ -band EMIC waves with the source amplification region expanded to $\pm 11^{\circ}$ MLAT.				
1068					
1069 1070	Figure 4. Comparison between calculated and observed He $^+$ -band EMIC wave amplitudes ($\pm 5^\circ/\pm 10^\circ$ MLAT source region)				
1071	Caption: Same format as Figure 2 but showing the analysis for the He ⁺ -band EMIC waves.				
1072					
1073 1074	Figure 5. Comparison between calculated and observed He ⁺ -band EMIC wave amplitudes (±11 MLAT source region)				
1075	Caption : Same format as Figure 3 but showing the analysis for the He ⁺ -band EMIC waves.				
1076					
1077	Figure 6. Inner magnetosphere A_{hp} distributions				
1078 1079	Caption: The measured hot proton anisotropy during all periods where $\Sigma_h - S_h > 0$ (a) and during periods of $\Sigma_h - S_h > 0$ which coincide with EMIC waves (b).				
1080					
1081	Figure 7. A_{hp} amplification factors				
1082 1083	Caption: Same format as Figure 2 but showing the necessary multiplicative A_{hp} factors needed for the (a) H ⁺ -band and (b) He ⁺ -band calculations to match observations.				
1084					
1085					
1086					
1087					
1088					
1089					
1090					
1091					
1092	Figures:				

1093	Figure	1.
1000	riguit	1.



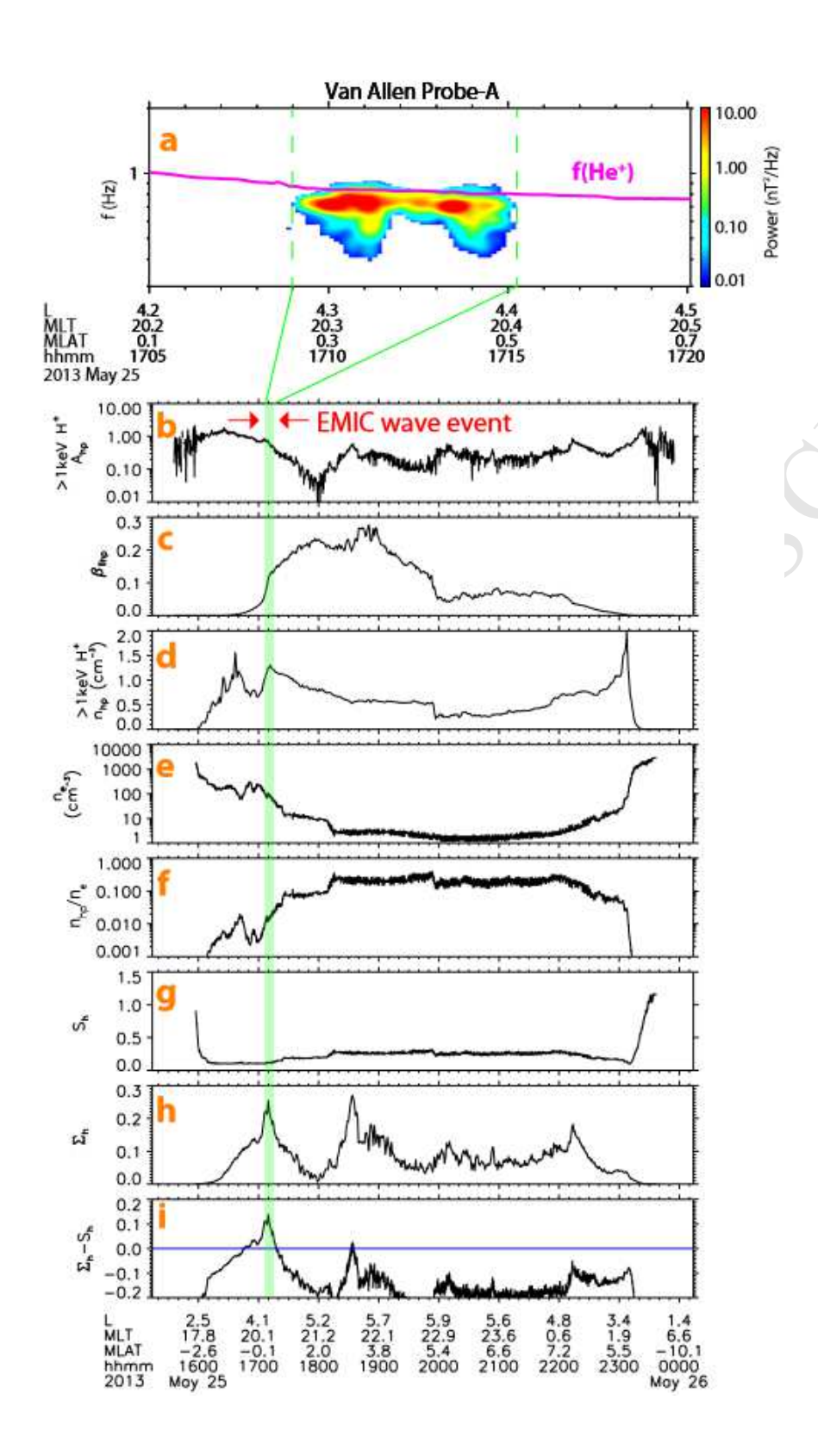


Figure 2.

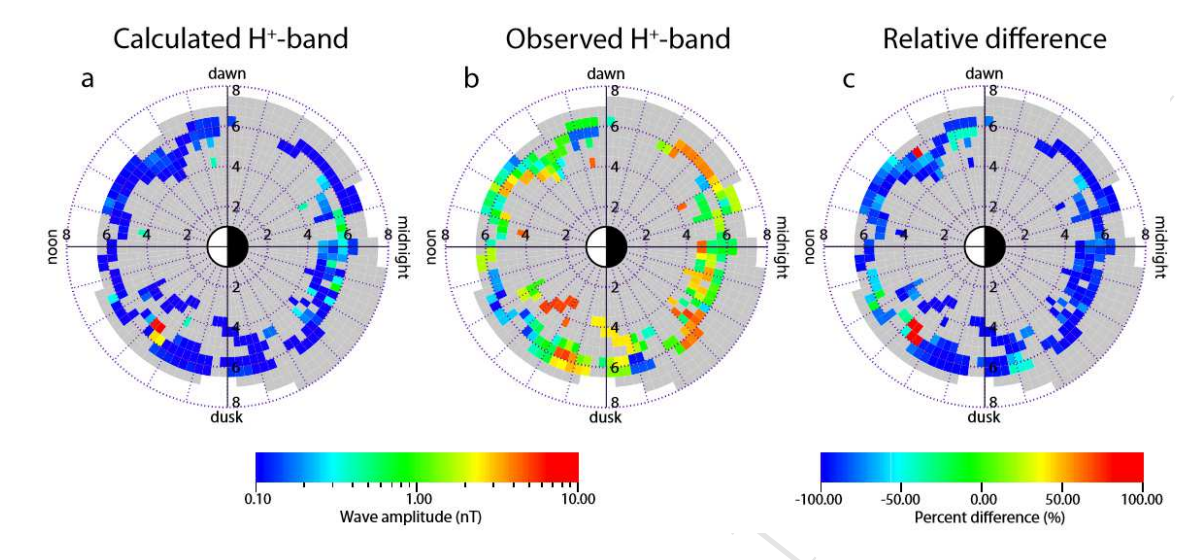


Figure 3.

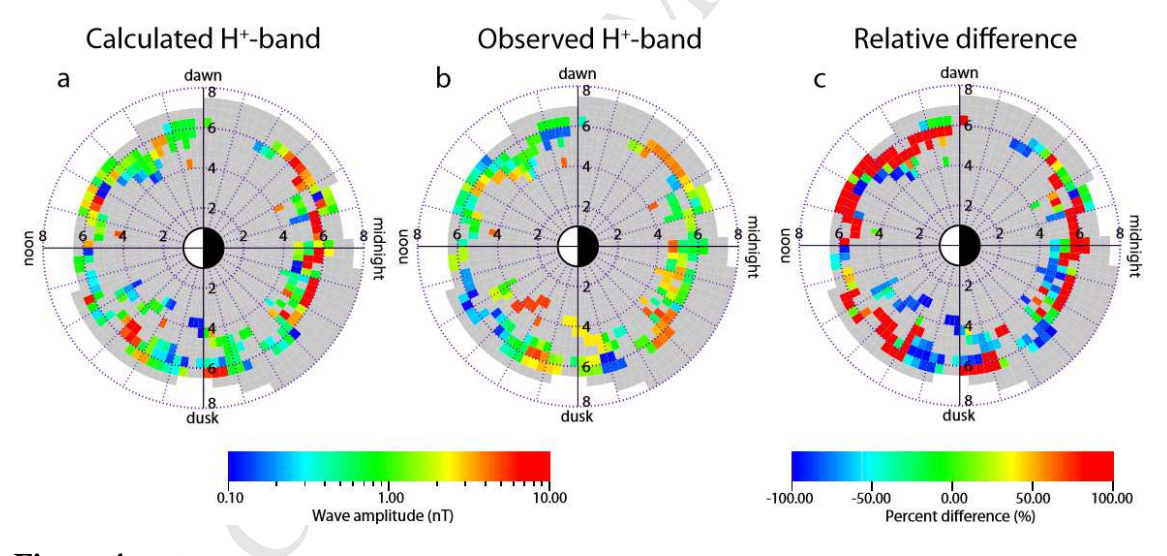


Figure 4.

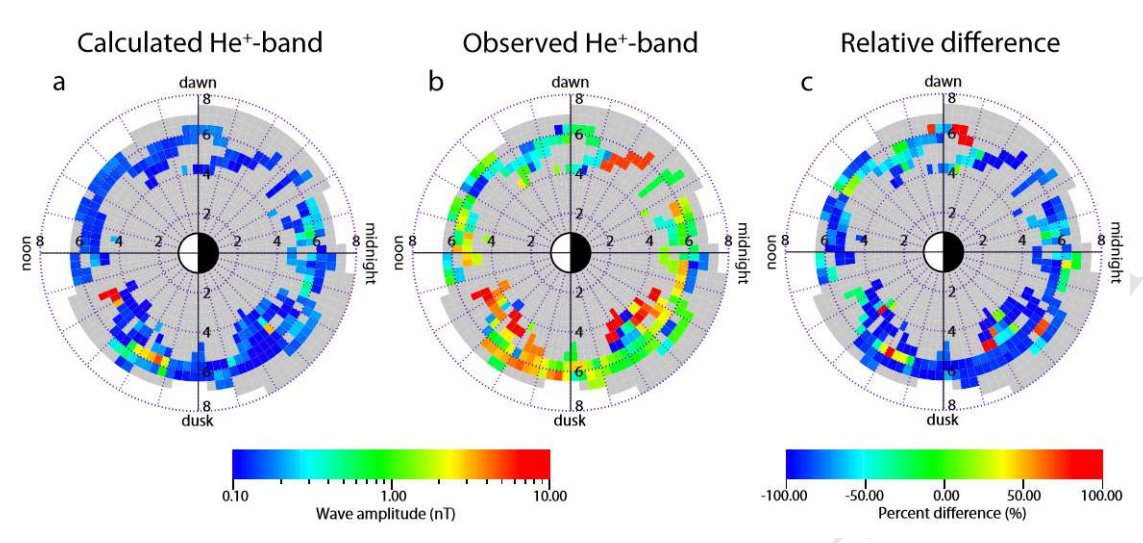
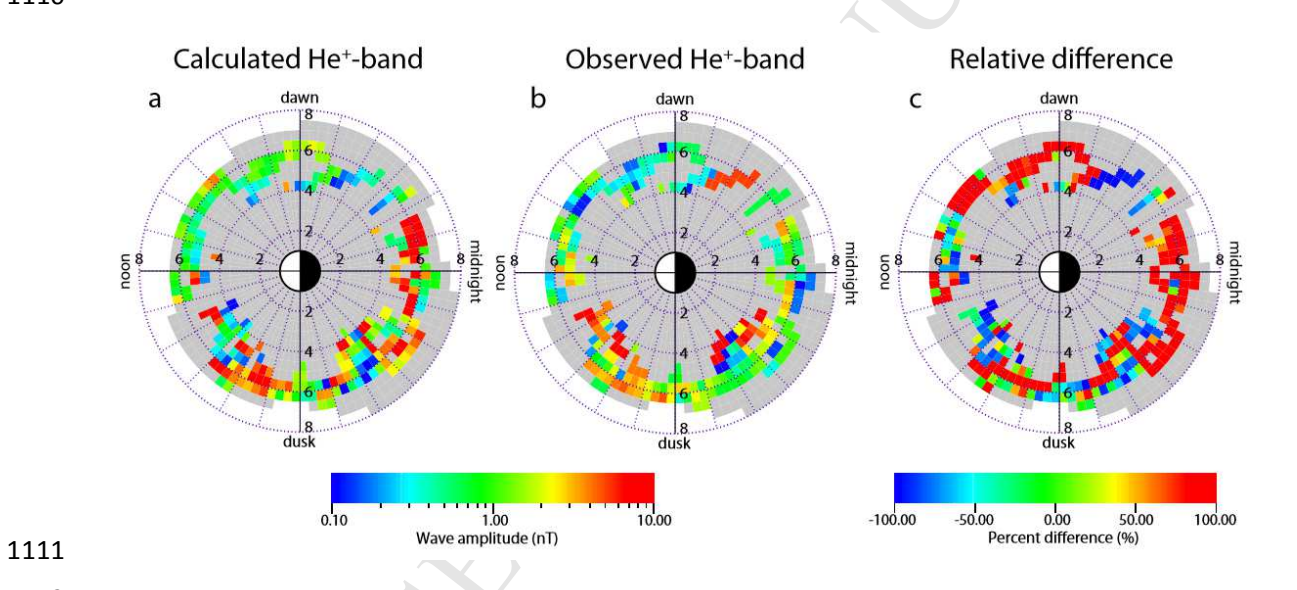
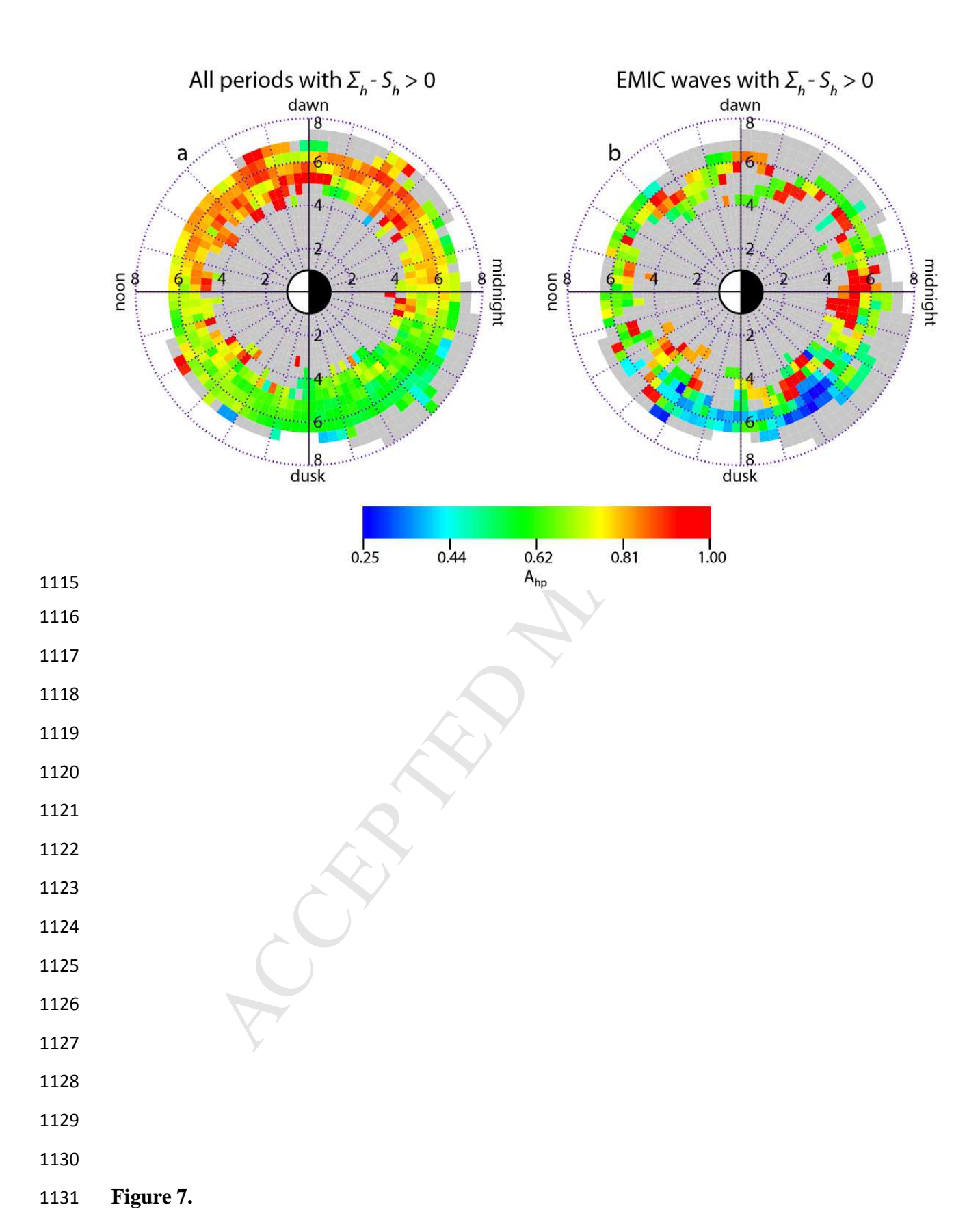
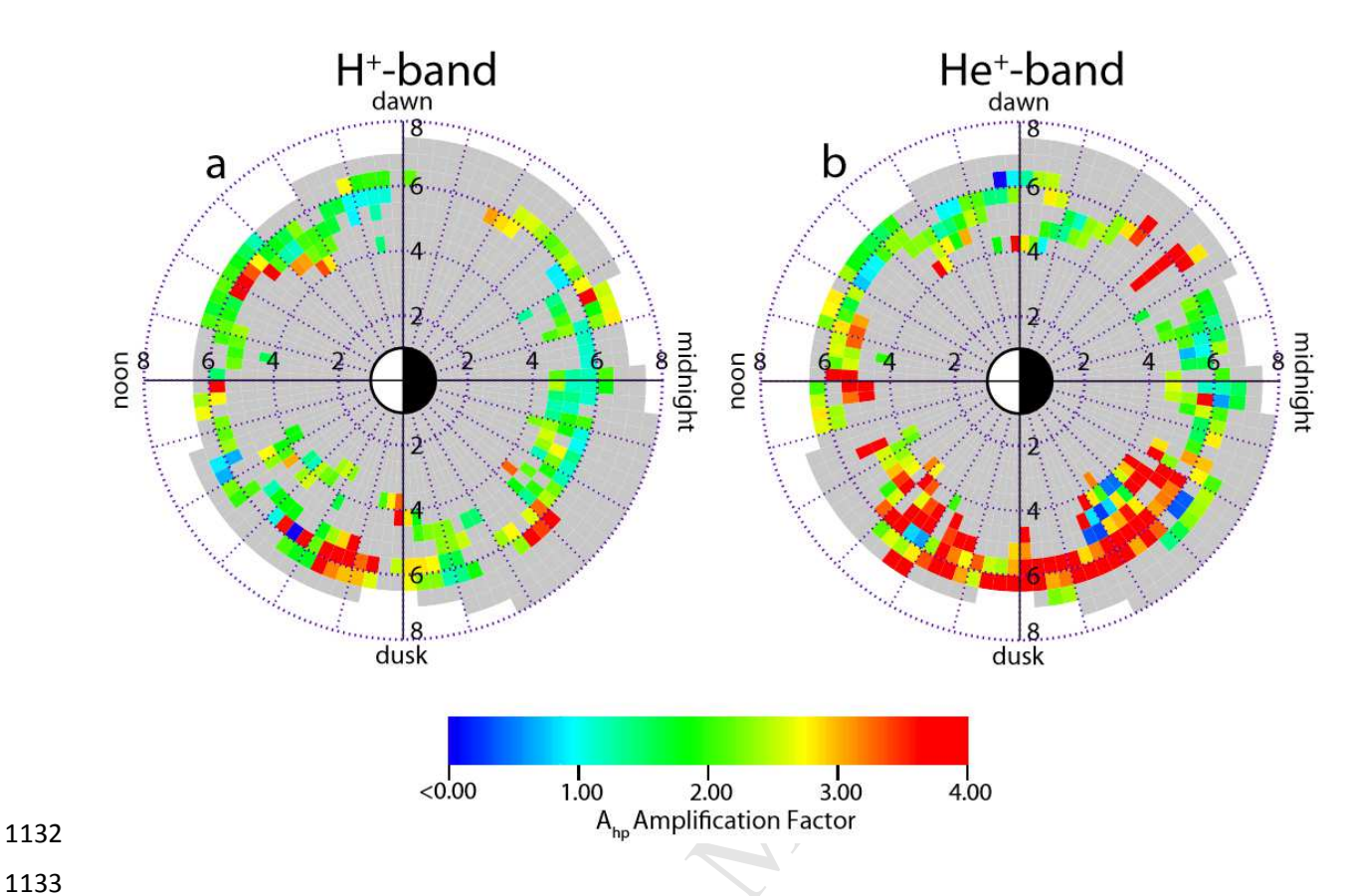


Figure 5.



1114 Figure 6.





Tables:

Table 1. Percentages of EMIC wave events with simulated wave amplitudes within ± 0.1 nT of the observed wave amplitudes after A_{hp} , A_{hhe} , and A_{ho} are altered, exclusively.

Wave Band	$A_{hp}*$	$A_{hhe}*$	$A_{ho}*$
H ⁺ -band	75.5%	11.8%	10.8%
He ⁺ -band	73.4%	20.2%	20.2%

*Denotes that the ion anisotropy has been altered.